The drag exerted by weakly dissipative trapped lee waves on the atmosphere: application to Scorer's two-layer model

Received: 12 April 2022 | Revised: 23 July 2022 | Accepted: 29 July 2022 | Published on: 29 September 2022

DOI: 10.1002/qj.4355

Quarterly Journal of the Royal Meteorological Society RMetS

RESEARCH ARTICLE

The drag exerted by weakly dissipative trapped lee waves on the atmosphere: Application to Scorer's two-layer model

Miguel A. C. Teixeira[1] | **José L. Argaín**[2,3]

[1]Department of Meteorology, University of Reading, Reading, UK

[2]Department of Physics, University of Algarve, Faro, Portugal

[3]CIMA, University of Algarve, Faro, Portugal

Correspondence
M. A. C. Teixeira, Department of Meteorology, University of Reading, Reading, Berkshire RG6 6ET, UK.
Email: m.a.teixeira@reading.ac.uk

Abstract

Although it is known that trapped lee waves propagating at low levels in a stratified atmosphere exert a drag on the mountains that generate them, the distribution of the corresponding reaction force exerted on the atmospheric mean circulation, defined by the wave momentum flux profiles, has not been established, because for inviscid trapped lee waves these profiles oscillate indefinitely downstream. A framework is developed here for the unambiguous calculation of momentum flux profiles produced by trapped lee waves, which circumvents the difficulties plaguing the inviscid trapped lee wave theory. Using linear theory, and taking Scorer's two-layer atmosphere as an example, the waves are assumed to be subject to a small dissipation, expressed as a Rayleigh damping. The resulting wave pattern decays downstream, so the momentum flux profile integrated over the area occupied by the waves converges to a well-defined form. Remarkably, for weak dissipation, this form is independent of the value of Rayleigh damping coefficient, and the inviscid drag, determined in previous studies, is recovered as the momentum flux at the surface. The divergence of this momentum flux profile accounts for the areally integrated drag exerted by the waves on the atmosphere. The application of this framework to this and other types of trapped lee waves potentially enables the development of physically based parametrizations of the effects of trapped lee waves on the atmosphere.

KEYWORDS

gravity wave drag, linear wave theory, mountain waves, wave momentum flux, wave trapping, weak dissipation

1 | INTRODUCTION

Orographic internal gravity waves in a stratified atmosphere (also known as mountain waves) exert a pressure drag on the mountains that generate them. By Newton's third law, a reaction force of equal magnitude and opposite direction must be exerted by the mountains on the atmosphere (Nappo, 2012). Since air is a fluid, this reaction force may be distributed spatially, in some cases over large distances, either vertically or horizontally. The mountains that act as a source of these waves have typical widths of order 10 km or smaller, and usually they are not resolved explicitly in weather prediction or climate models, so the waves must be parametrized (Stensrud, 2009). The total value of the orographic gravity wave drag and its spatial distribution need to be specified in such parametrizations (e.g., Lott and Miller, 1997).

A theory for the generation and dissipation of hydrostatic gravity waves, which propagate vertically in the atmosphere, has been extensively developed over the last decades (Phillips, 1984; McFarlane, 1987; Shutts, 1995; Shutts and Gadian, 1999), and serves as the physical basis for existing orographic gravity wave drag parametrizations. In this theory, where the linear approximation is typically made, the total drag can often be calculated analytically (Smith, 1979; Phillips, 1984; Teixeira *et al.*, 2004; Teixeira and Miranda, 2006), and even the distribution of the force exerted on the atmosphere, which is specified through the divergence of the vertical flux of horizontal wave momentum, can sometimes be expressed analytically (Shutts, 1995; Shutts and Gadian, 1999; Teixeira and Miranda, 2009; Teixeira and Yu, 2014). This tractability results from the simplifications inherent to the linear and hydrostatic approximations, whereby the waves not only are always vertically propagating, but are also absorbed by critical levels in an inviscid context via a mechanism that mimics their more realistic (finite-amplitude) attenuation by wave breaking (Booker and Bretherton, 1967; Shutts, 1995; Grubišić and Smolarkiewicz, 1997; Teixeira *et al.*, 2008). For stationary waves, critical levels can be defined as levels in the atmosphere where the mean wind velocity is perpendicular to the horizontal wave-number vector of the wave, or is simply zero. Since the mean wind vector is likely to turn substantially with height, or vanish, over the depth of the atmosphere, critical levels are an effective mechanism for momentum transfer from the waves to the mean flow. Other mechanisms that lead to an increase in the amplitude of the waves as their energy propagates upward, and therefore to their breaking and dissipation, with momentum transfer to the mean flow, are the decrease of density and variation of static stability with height (Smith, 1979; McFarlane, 1987). In hydrostatic waves, which propagate essentially vertically, the occurrence of any of these factors in an atmospheric column over the source orography will ensure that the wave momentum flux is totally deposited into the mean flow as the reaction force acting on the atmosphere.

However, the situation is less clear for trapped lee waves, and non-hydrostatic waves in general, whose properties have received much less attention (Xu *et al.*, 2021). Untrapped non-hydrostatic waves, if they are evanescent, produce no drag, and therefore no wave momentum flux (Teixeira *et al.*, 2013a). Vertically propagating non-hydrostatic waves, although producing a progressively smaller drag as the width of their source orography decreases (Xu *et al.*, 2021), are subject to the same dissipation mechanisms as hydrostatic waves, and the traditional version of the Eliasen–Palm theorem applies to them. Trapped lee waves, however, are different. They are intrinsically non-hydrostatic mountain waves that propagate horizontally in the atmosphere, as a result of vertical reflection and trapping (leading to ducting) within a layer, typically adjacent to the ground (Scorer, 1949; Vosper *et al.*, 2006). Analytical expressions for the total drag produced by these waves have been derived and tested, both for generic cases (Bretherton, 1969; Smith, 1976; Gregory *et al.*, 1998) and for waves propagating in simple two-layer atmospheres (Teixeira *et al.*, 2013a; 2013b; Teixeira and Miranda, 2017). These waves are expected to be dissipated primarily via friction within the boundary layer, as their energy repeatedly propagates towards the ground and is reflected by it (Jiang *et al.*, 2006; Lott, 2007), but there is no clear idea of how the divergence of the wave momentum flux may exert drag on the mean flow in that case. The reason is that, unlike in inviscid linear theory, where critical levels or the decay of density with height provide natural ways of producing a momentum flux divergence, there is no such mechanism for waves that propagate horizontally. Additionally, the inviscid solution from linear theory for trapped lee waves produces momentum fluxes that are both horizontal and vertical (Broad, 2002) and that are ill-defined, oscillating with the wave phase of the (horizontally infinite) wave train. There have been attempts to analyse the impact of trapped lee waves on the atmosphere with recourse to the theory proposed by Broad (2002) or the concept of wave pseudo-momentum (Shepherd, 1990), but progress has been limited by the fact that a non-dissipative framework was adopted (Durran, 1995; Lott, 1998; Xue *et al.*, 2022). Very recently, Soufflet *et al.* (2022) (following Lott, 2007) assumed a diffusive representation of friction in the boundary layer to calculate the momentum fluxes associated with trapped lee waves but did not explore the limit of zero friction, which makes an interpretation of their results difficult.

As will be seen in this study, in order to obtain a well-posed mathematical problem for the trapped lee waves (even restricted to linear theory) that allows a derivation of the effect of the waves on the mean flow through the momentum flux divergence terms in the equations of motion, it is necessary to introduce at least weak dissipation. The corresponding treatment provides an example of a situation in a fluid flow in which the limit of the solution when friction approaches zero is different from the solution when friction is assumed from the outset to be exactly zero, and physically meaningful results are only obtained in the former case. This parallels

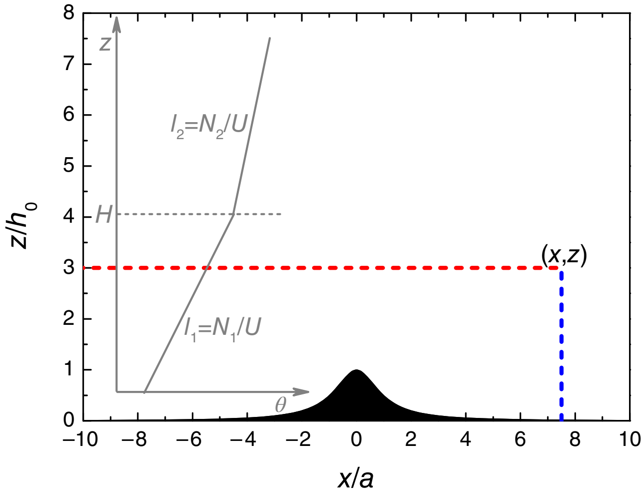

FIGURE 1 Diagram showing the isolated mountain (with height h_0 and half-width a) that generates the trapped lee waves (in black) and the lines along which the momentum fluxes are integrated to obtain P_z (red dashed line) and P_x (blue dashed line) according to Equation (20). (x, z) is a generic point defining the upper limits of integration of P_x and P_z. The mean flow is assumed to come from the left. The graph in the inset describes the potential temperature θ profile for the two-layer atmosphere of Scorer. $l_1 = N_1/U$ and $l_2 = N_2/U$ are the Scorer parameters in the lower and upper layer respectively (where N_1 and N_2 are the corresponding Brunt–Väisälä frequencies and U is the (constant) wind speed. The separation between the two layers is at $z = H$. [Colour figure can be viewed at wileyonlinelibrary.com]

the mechanisms in boundary-layer theory that resolve D'Alembert's paradox, and in other fluid dynamics problems involving the effects of weak friction (e.g., Teixeira *et al.*, 2012).

In this study, the simplest representation of friction as a Rayleigh damping will be adopted, and results will be illustrated for the case of the two-layer atmosphere of Scorer (Scorer, 1949; Teixeira *et al.*, 2013a) (see Figure 1), but the results are found to be independent of the value of the Rayleigh damping coefficient, as long as this is small, and the concept underlying the calculations appears to be generalizable to other model atmospheres. The independence of the results from the details of the Rayleigh damping suggest, in particular, that they may be independent of the type of dissipation adopted (as long as this is weak), and probably constitute the true quasi-inviscid solution to the momentum flux profiles that may serve as a leading-order orographic forcing in gravity wave drag parametrizations.

This article is organized as follows: Section 2 describes theoretical developments, including an extension of inviscid results, results with weak friction, and their application to Scorer's atmosphere. Section 3 presents the nonlinear numerical model and the linear model with friction against which the theory is compared. Section 4 presents some preliminary comparisons, both purely inviscid and with vanishing friction, used to validate the theoretical results. Finally, Section 5 summarizes the main conclusions of this study.

2 | THEORY

In view of the difficulties pointed out, the existing theory for the momentum fluxes associated with trapped lee waves can be considered unsatisfactory and incomplete. Since basic aspects still need attention, the present treatment will be limited to conditions under which two-dimensional (2D) linear theory is valid, and a brief review of previous results is included in the theoretical development.

For vertically propagating waves, the effect of the waves on the mean flow (which in a parametrization corresponds to the resolved atmospheric circulation) is given by (cf. Stensrud, 2009; Nappo, 2012)

$$\rho \frac{\partial \langle U \rangle}{\partial t} = -\frac{\partial}{\partial z}(\rho \langle uw \rangle) + \text{other terms}, \tag{1}$$

where U is the mean wind velocity (in the x direction), u and w are respectively the horizontal and vertical velocity perturbations associated with the waves, and ρ is the density. The angle brackets denote the average over a certain area or (in two dimensions) spatial distance along x, say:

$$\langle uw \rangle = \frac{\int_{-\Delta x/2}^{+\Delta x/2} uw \, dx}{\Delta x}. \tag{2}$$

In Equation (1), the nonlinear term explicitly presented on the right-hand side inside the z derivative is the wave momentum flux, which causes a deceleration (or acceleration) of the mean flow. In Equation (2), Δx may represent, for example, the grid spacing along x in the model where the drag parametrization is implemented. Implicit in the terms omitted in Equation (1) is the idea that the contribution to the drag from the divergence of the horizontal momentum fluxes is irrelevant, as those fluxes become zero at the edges of the integration domain used in Equation (2). This is consistent with vertically propagating (hydrostatic) waves generated by an isolated mountain, which justify a so-called "single-column" approach to drag parametrization.

In the theory of internal gravity waves generated by isolated mountains that serves as a basis for most drag parametrizations, what is called the wave momentum flux is often denoted by

$$M = \rho \int_{-\infty}^{+\infty} uw\, dx, \tag{3}$$

or the corresponding 2D integral version for three-dimensional flow (Bretherton, 1969; Shutts, 1995; Teixeira and Miranda, 2009; Teixeira and Yu, 2014). The definition of Equation (3) will be adopted here. Despite the fact that the integration limits in Equation (3) are different from those in Equation (2), if the waves are hydrostatic and generated by an isolated mountain then the integral should take the same value. From inviscid linear wave theory, it can be shown (Smith, 1979; Teixeira and Miranda, 2009; Nappo, 2012) that

$$\begin{aligned} M(z=0) &= \rho \int_{-\infty}^{+\infty} uw(z=0)\, dx \\ &= -\int_{-\infty}^{+\infty} p(z=0)\frac{\partial h}{\partial x}\, dx = -D, \end{aligned} \tag{4}$$

where p is the pressure perturbation associated with the waves and $h(x)$ is the terrain elevation. D is the total drag exerted by the atmosphere on the orography. This can be viewed as an expression of Newton's third law.

It is clear from Equation (1) that the vertical profile of $\rho\langle uw\rangle$, or equivalently of M, is crucial to define the drag exerted on the atmosphere by orographic gravity waves. However, difficulties arise when one attempts to evaluate M for trapped lee waves. Since the wave solutions are most conveniently expressed in Fourier space, one might think that a way to evaluate M would be by applying Parseval's theorem to the definition of momentum flux in physical space (Bretherton, 1969; Teixeira and Miranda, 2009; Nappo, 2012), which for horizontally bounded waves yields from Equation (3)

$$M = 2\pi \mathrm{i} \rho \int_{-\infty}^{+\infty} \hat{u}^* \hat{w}\, dk, \tag{5}$$

where k is the horizontal wave number, $\hat{u}$ and $\hat{w}$ are the one-dimensional Fourier transforms of u and w, the asterisk denotes complex conjugate, and $\mathrm{i} = \sqrt{-1}$. Unfortunately, Equation (5) cannot be used for inviscid trapped lee waves, at least when $z > 0$, because u and w do not approach zero downstream of the mountain as $x \to +\infty$ (and hence their Fourier integrals [in x] do not converge). The momentum flux profile must, therefore, be obtained from an independent constraint, which generalizes Eliassen–Palm's theorem (Eliassen and Palm, 1960; Broad, 2002). This constraint can be derived in two alternative ways: either from direct manipulation of the equations of motion, or as a consequence of the conservation of wave activity under steady conditions (Shepherd, 1990; Lott, 1998). These two results will emerge as special cases of the more general treatment, including friction, to be presented next.

Consider the steady, linearized equations of motion for adiabatic 2D flow with the Boussinesq approximation (cf. Teixeira *et al.*, 2012):

$$U\frac{\partial u}{\partial x} + w\frac{dU}{dz} = -\frac{1}{\rho_0}\frac{\partial p}{\partial x} - \lambda u, \tag{6}$$

$$U\frac{\partial w}{\partial x} = -\frac{1}{\rho_0}\frac{\partial p}{\partial z} + b - \lambda w, \tag{7}$$

$$U\frac{\partial b}{\partial x} + N^2 w = 0, \tag{8}$$

$$\frac{\partial u}{\partial x} + \frac{\partial w}{\partial z} = 0, \tag{9}$$

where $b = g\theta'/\theta_0$ is the buoyancy perturbation associated with the waves, g is the gravitational acceleration, θ' is the potential temperature perturbation, and θ_0 is a reference potential temperature (assumed to be constant). N^2 is the static stability of the mean incoming flow, and ρ_0 is a reference density (assumed to be constant). In this equation set, Rayleigh friction, with a (constant) damping coefficient λ, has been introduced only in the momentum balance equations, for simplicity—for a justification of this choice, see Teixeira *et al.* (2012).

If Equation (6) is multiplied by u and Equation (7) is multiplied by w and both equations are added, this yields

$$\begin{aligned} &U\frac{\partial}{\partial x}\left(\frac{u^2+w^2}{2}\right) + uw\frac{dU}{dz} + \frac{\partial}{\partial x}\left(\frac{pu}{\rho_0}\right) + \frac{\partial}{\partial z}\left(\frac{pw}{\rho_0}\right) \\ &\quad + N^2\zeta w + \lambda\left(u^2+w^2\right) = 0, \end{aligned} \tag{10}$$

where ζ is the vertical displacement of isentropes (or streamlines), which satisfies $w = U\partial\zeta/\partial x$; Equation (9) has been used, and a version of Equation (8) integrated with respect to x, yielding $b = -N^2\zeta$, has also been used. Equation (6) may also be integrated with respect to x, yielding

$$Uu + U\frac{dU}{dz}\zeta + \frac{p}{\rho_0} + \lambda \int^x u\, dx = 0. \tag{11}$$

This equation may be multiplied by u or w, and differentiated with respect to x or z respectively, to eliminate the pressure terms in Equation (10). When this is done, some terms cancel out (see Appendix A), and the following equation is obtained:

$$U\frac{\partial}{\partial x}\left[\frac{w^2-u^2}{2}+\frac{1}{2}\left(N^2-U\frac{d^2U}{dz^2}\right)\zeta^2\right] - U\frac{\partial}{\partial z}(uw)-\lambda w\int^x\left(\frac{\partial u}{\partial z}-\frac{\partial w}{\partial x}\right)dx=0. \tag{12}$$

When friction is neglected, and Equation (12) is multiplied by $-\rho_0/U$, it takes the simpler form

$$-\frac{\partial}{\partial x}\left[\rho_0\frac{w^2-u^2}{2}+\frac{1}{2}\rho_0\left(N^2-U\frac{d^2U}{dz^2}\right)\zeta^2\right] + \frac{\partial}{\partial z}(\rho_0 uw)=0. \tag{13}$$

If this equation is integrated between $x=-\infty$ and a generic $x>0$ (assuming that any existing orography is isolated and centred at $x=0$), the following results:

$$\frac{\partial}{\partial z}\left(\rho_0\int_{-\infty}^{x}uw\,dx\right) = \left[\rho_0\frac{w^2-u^2}{2}+\frac{1}{2}\rho_0\left(N^2-U\frac{d^2U}{dz^2}\right)\zeta^2\right](x), \tag{14}$$

where the fact that no wave perturbations exist as $x\to-\infty$ (i.e., upstream of the mountain) has been used. If d^2U/dz^2 is neglected, Equation (14) can be shown to be equivalent to eq. (10) of Broad (2002). Broad (2002) then chose to focus on a value of x corresponding to a phase of the trapped lee waves where both u and ζ are zero—note that u and ζ are in phase because $u=-(\partial/\partial z)(U\zeta)$, from $w=U\partial\zeta/\partial x$ and mass conservation, Equation (9). With these simplifications, Equation (14) reduces to eq. (15) of Broad (2002) (where only the term involving w^2 on the right-hand side remains). It is not obvious, however, why this phase of the trapped lee wave should be privileged. Clearly, there is no unique limit for Equation (14) when $x\to+\infty$; so, according to Equation (3), M is mathematically ill-defined.

Another way to arrive at Equation (14) is using the wave activity balance equation (Shepherd, 1990; Lott, 1998). For a steady flow, the wave activity balance for 2D gravity waves with the Boussinesq approximation may be written

$$\frac{\partial F_x}{\partial x}+\frac{\partial F_z}{\partial z}=0, \tag{15}$$

where

$$F_x=\frac{\rho_0 U}{N^2}b\left(\frac{\partial u}{\partial z}-\frac{\partial w}{\partial x}\right)+\frac{1}{2}\frac{\rho_0}{N^4}\left(N^2-U\frac{d^2U}{dz^2}\right)b^2 - \rho_0\left(\frac{w^2-u^2}{2}\right),\qquad F_z=\rho_0 uw; \tag{16}$$

compare with Lott (1998, eqs. 23–25) or the left-hand side of eq. (10) of Soufflet *et al.* (2022). Equation (15) expresses the fact that the divergence of the (2D) pseudomomentum vector (F_x,F_z) is zero. Using the equalities $b=-N^2\zeta$, $w=U\partial\zeta/\partial x$, and $u=-(\partial/\partial z)(U\zeta)$, F_x may be expressed as

$$F_x=\rho_0U^2\zeta\left(\frac{\partial^2\zeta}{\partial x^2}+\frac{\partial^2\zeta}{\partial z^2}+\frac{2}{U}\frac{dU}{dz}\frac{\partial\zeta}{\partial z}+\frac{N^2}{U^2}\zeta\right) - \left[\rho_0\frac{w^2-u^2}{2}+\frac{1}{2}\rho_0\left(N^2-U\frac{d^2U}{dz^2}\right)\zeta^2\right]. \tag{17}$$

The expression in the first set of parentheses in this equation is zero—from the equation governing the behaviour of linear gravity waves; see Lin (2007) (eq. 5.3.1). This shows that Equation (15) is actually equivalent to Equation (13); that is, the first term in parentheses in Equation (13) is minus a simplified form of the x component of the pseudomomentum vector. As far as we are aware, this is the first time that this has been pointed out.

Lott (1998) noted that if Equation (15), or Equation (13), is integrated horizontally between $-\infty$ and a generic x (for x downstream of the mountain) and vertically between 0 and $z>0$, which is equivalent to integrating Equation (14) in the vertical between 0 and z, the following is obtained:

$$\rho_0\int_{-\infty}^{x}uw\,dx - \rho_0\int_0^z\left[\frac{w^2-u^2}{2}+\frac{1}{2}\left(N^2-U\frac{d^2U}{dz^2}\right)\zeta^2\right]dz = \rho_0\int_{-\infty}^{x}uw(z=0)\,dx, \tag{18}$$

or in a more compact form

$$P_x+P_z=P_z(z=0), \tag{19}$$

where

$$P_x=\int_0^z F_x\,dz,\quad P_z=\int_{-\infty}^{x}F_z\,dx, \tag{20}$$

as defined by Lott (1998) or Soufflet *et al.* (2022). Equation (18), or Equation (19), shows that the sum of the integrated pseudomomentum fluxes along x and along z adds up to a constant value, which is equal to the vertical flux of horizontal pseudomomentum (or momentum) at the surface—by Equation (4), this is additionally equal (in value) to the surface pressure drag. In Figure 1, the horizontal red dashed line shows the domain of integration of P_z and the vertical blue dashed line is the domain of integration of P_x. Clearly, any momentum flux emanating from the mountain (in black) must cross one of these lines. Equation (18) suggests that inviscid linear theory cannot tell anything useful about the way the wave momentum fluxes force the mean flow, as this would require a depletion of the total integrated wave pseudo-momentum flux. In order to make progress, it is necessary to go back to Equation (12), which includes friction. Taking Equations (16) and (17) into account (see also Appendix A), Equation (12) can be considered equivalent to eq. (10) of Soufflet *et al.* (2022), with the difference that the representation of friction on the right-hand side is more simplified. Soufflet *et al.* (2022) represent friction as a vertical diffusion that also affects heat instead of a Rayleigh damping affecting only momentum.

If Equation (12) is integrated horizontally between $-\infty$ and $+\infty$, the first term with the x derivative now cancels out, because when friction is included the trapped lee waves decay to zero downstream over a longer or shorter distance. Hence, this integration yields

$$\frac{\partial}{\partial z}\int_{-\infty}^{+\infty} uw\, dx = \lambda \int_{-\infty}^{+\infty} \zeta \left(\frac{\partial u}{\partial z} - \frac{\partial w}{\partial x}\right) dx, \tag{21}$$

where $w = U\partial\zeta/\partial x$ has been used, Equation (12) has been divided by U, and the frictional term has been integrated by parts (see Appendix A). Equation (21) expresses the fact that the divergence of the wave momentum flux is balanced by downstream dissipation of the waves due to friction. To obtain the vertical momentum flux itself (which is the only one relevant in this problem, as the horizontal momentum flux decays to zero downstream with the waves), Equation (21) needs to be integrated in the vertical, but now between a generic z and $+\infty$ (where the uw associated with the waves is zero). Note that this implies that only trapped lee waves, which by definition decay to zero as $z \to +\infty$, are being considered. This yields

$$\int_{-\infty}^{+\infty} uw\, dx = -\lambda \int_{z}^{+\infty}\int_{-\infty}^{+\infty} \zeta \left(\frac{\partial u}{\partial z} - \frac{\partial w}{\partial x}\right) dx\, dz. \tag{22}$$

When friction is included (as is the case in the present treatment), the wave equation used to simplify Equation (17), which can be derived from the original equation set (Equations 6–9), becomes more complicated, having some additional terms involving λ. However, in the limit of weak friction, it still takes approximately the same form. In this approximation, which amounts to neglecting any terms proportional to powers of λ higher than 1, Equation (22) may also be written as (see Appendix A)

$$\int_{-\infty}^{+\infty} uw\, dx = -\lambda \int_{z}^{+\infty} \frac{1}{U}\left(N^2 - U\frac{d^2U}{dz^2}\right)\int_{-\infty}^{+\infty} \zeta^2\, dx\, dz. \tag{23}$$

Clearly, under the necessary condition for vertical wave propagation, $N^2 - Ud^2U/dz^2 > 0$, which is required for wave trapping to occur in a layer, the term on the right-hand side of Equation (23) will always be negative, which means that the momentum flux will equally be negative, and approach zero at high levels. This makes sense, since the waves are trapped within a layer, and $uw(z = 0)$ should be negative by Newton's third law. In their studies on the diurnal evolution of trapped lee waves, Xue and Giorgietta (2021) and Xue *et al.* (2022) assume that the total momentum flux associated with trapped lee waves is zero (a consequence of their eqs 7 and 9 respectively). This results from the fact that, in the absence of a theory including friction, Xue and co-workers (Xue and Giorgietta, 2021; Xue *et al.*, 2022) inconsistently apply the inviscid theory of Broad (2002) to numerical simulation results where the trapped lee waves decay in space. Equation (23) corrects this inconsistency. Note that, in the term on the right-hand side of Equation (23), both N and U may vary with height, so they were kept inside the vertical integral. Also worthy of note is that this term involves integrals over the whole wave field (in the horizontal and in the vertical directions). Therefore, the form and variation of uw with height is a global property of the wave field (in particular, horizontally, from its point of generation to its point of total dissipation). It is this vertical flux of horizontal momentum that forces the mean flow in the area over the trapped lee wave field. Although, from Equation (23), the momentum flux apparently should depend on λ, it actually does not, at least for low values of that parameter, as will be shown next. This is not obvious from Equation (23), but may be understood intuitively in a qualitative way. The smaller λ is, the more slowly the wave field spanned by the horizontal integral in Equation (23) is expected to decay with x, therefore yielding a larger integral. It is plausible that these two effects could potentially cancel.

Interestingly, for weak friction, Equation (4) remains approximately valid. This can be shown departing from Equation (11). If Equation (11) is multiplied by w and integrated horizontally between $-\infty$ and $+\infty$, the result is the following:

$$U\int_{-\infty}^{+\infty} uw\, dx + \frac{1}{\rho_0}\int_{-\infty}^{+\infty} pw\, dx - \lambda U \int_{-\infty}^{+\infty} u\zeta\, dx = 0, \tag{24}$$

where $w = U\partial\zeta/\partial x$ has been used, the term coming from the second term of Equation (11) vanishes, because it can be expressed as the horizontal integral of $(1/2)U^2(dU/dz)\partial(\zeta^2)/\partial x$, and the last term has been integrated by parts. If Equation (24) is multiplied by ρ_0/U and applied at $z = 0$, it becomes

$$\rho_0\int_{-\infty}^{+\infty} uw(z=0)\, dx + \int_{-\infty}^{+\infty} p(z=0)\frac{\partial h}{\partial x}\, dx - \lambda\rho_0\int_{-\infty}^{+\infty} uh\, dx = 0, \tag{25}$$

where $w(z=0)=\partial h/\partial x$ and $\zeta(z=0)=h$ have been used. Since h is only non-zero near to the orography (which is assumed to be isolated), the integral on the last term does not increase indefinitely as λ decreases, and therefore the whole term vanishes as $\lambda \to 0$—unlike the last term in Equation (23). Therefore, the conclusion is that Equation (4) still holds, as intended.

2.1 | Application to Scorer's atmosphere

Equation (23) is the main outcome of the preceding section. It describes the variation of the vertical flux of horizontal momentum associated with the trapped lee waves under the linear approximation, representing frictional effects as a Rayleigh damping. In order to proceed further, it is necessary to assume a specific atmospheric profile, which will determine the form of ζ inside the integral on the right-hand side of Equation (23). A crucial question is how to specify ζ itself. Clearly, in order for the integrals on the right-hand side of Equation (23) to converge, the wave field must be bounded (which is consistent with the existence of friction). Analytical expressions for ζ (in physical space) in trapped lee waves with friction do not exist, even under the linear approximation (Jiang *et al.*, 2006; Smith *et al.*, 2006). Asymptotic solutions for ζ (downstream of the mountain) from inviscid linear theory are analytical (Scorer, 1949; Mitchell *et al.*, 1990), but they (accurately) extend indefinitely in space; so, if they were used in Equation (23) without adaptation, the horizontal integral on the right-hand side would not converge. Here, a compromise will be made, which can be shown to be increasingly accurate as λ becomes smaller: the inviscid solutions for ζ will be used, but multiplied by an exponentially decaying factor that accounts for the effect of weak friction. This seems a very reasonable approach, since for the calculation of the right-hand side of Equation (23) the primary effect of weak friction is to limit the wave field to a finite extent in space but, apart from this modulation, the solution for ζ is virtually indistinguishable from the inviscid one.

More specifically, it will be assumed that

$$\zeta = \zeta_{\mathrm{inv}} \; \mathrm{e}^{-k_{\mathrm{I}}x}, \tag{26}$$

where ζ_{inv} is the inviscid form of ζ, and k_{I} is the imaginary part of the wave number associated with a spectral representation of ζ. Whereas $k_{\mathrm{I}}=0$ for an inviscid solution, $k=k_{\mathrm{R}}+\mathrm{i}k_{\mathrm{I}}$ in the solution with friction. For all purposes, in what follows it will be assumed that $k=k_{\mathrm{R}}$, and k_{I} will be assumed to be non-zero, but very small, in Equation (26) via a definition to be presented, relating k_{I} to λ. For the time being, it is sufficient to recognize that Equation (26) is accurate. Inserting Equation (26) into Equation (23) yields

$$\int_{-\infty}^{+\infty} uw \, dx = -\lambda \int_{0}^{+\infty} \int_{z}^{+\infty} Ul^2 \zeta_{\mathrm{inv}}^2 \, dz \, \mathrm{e}^{-2k_{\mathrm{I}}x} \, dx, \tag{27}$$

where $l=[N^2/U^2-(1/U)(d^2U/dz^2)]^{1/2}$ is the Scorer parameter. For convenience, the integrations over x and z have been swapped (note that the exponential term does not depend on z), and it has been noted that the trapped lee waves only exist downstream of the mountain (assumed to be centred at $x=0$), hence the lower limit of integration in x has been changed from $-\infty$ to 0. All of this ensures that the horizontal integral on the right-hand side of Equation (27) converges.

The inviscid solution ζ_{inv} for the two-layer atmosphere of Scorer (1949) is easily obtained from the corresponding solutions for the Fourier transforms of flow variables in Teixeira *et al.* (2013a), in the same way as this was done in Teixeira and Miranda (2017) for similar, but three-dimensional, waves. It is assumed here that not only is the Scorer parameter constant in each layer, but also that there is no wind shear and the wind speed in the two layers is equal. The solution corresponds to a monochromatic wave resulting from a singularity in the Fourier transform, as originally noted by Scorer (1949) (the same singularity that is responsible for the drag from trapped lee waves in Teixeira *et al.* (2013a)), and can be written

$$\begin{aligned}
\zeta_{\mathrm{inv}} &= -4\pi \frac{\hat{h}(k_{\mathrm{L}}) m_1(k_{\mathrm{L}}) n_2(k_{\mathrm{L}}) \sin[m_1(k_{\mathrm{L}})z]}{k_{\mathrm{L}}[1+n_2(k_{\mathrm{L}})H]} \sin(k_{\mathrm{L}}x) \\
&\quad \text{if } 0<z<H, \\
\zeta_{\mathrm{inv}} &= -\frac{4\pi}{(l_1^2-l_2^2)^{1/2}} \frac{\hat{h}(k_{\mathrm{L}}) m_1^2(k_{\mathrm{L}}) n_2(k_{\mathrm{L}}) \; \mathrm{e}^{-n_2(k_{\mathrm{L}})(z-H)}}{k_{\mathrm{L}}[1+n_2(k_{\mathrm{L}})H]} \sin(k_{\mathrm{L}}x) \\
&\quad \text{if } z>H,
\end{aligned} \tag{28}$$

where H is the height of the interface between the two layers and $\hat{h}$ is the Fourier transform of the terrain elevation h. k_{L} is the horizontal wave number of the resonant trapped lee wave mode, $m_1=(l_1^2-k^2)^{1/2}$ is the vertical wave number in the lower layer, and $n_2=(k^2-l_2^2)^{1/2}$ is the vertical spatial decay rate of the waves in the upper layer, where they are evanescent. $l_1=N_1/U$ and $l_2=N_2/U$ are the Scorer parameters in the lower and upper layers respectively, where N_1 and $N_2<N_1$ are the corresponding Brunt–Väisälä frequencies (since in Scorer's atmosphere $d^2U/dz^2=0$). Note that, unlike in Teixeira *et al.* (2013a) or Teixeira and Miranda (2017), a sum is not included in Equation (28) because the results will only focus on a single trapped lee wave mode (the lowest one), for simplicity. But, to be strictly correct, the sum over all wave modes should be included, as in Teixeira *et al.* (2013a). Strictly

speaking, the asymptotic solution of Equation (28) is only accurate beyond some distance downstream of the mountain ($x > 0$), as noted by Scorer (1949). But both use of this approximation in the calculation of the horizontal integral on the right-hand side of Equation (27) and the adoption of the lower limit of integration 0 (centred on the mountain), although subject to some errors for finite friction, are actually extremely accurate for weak friction. This is because, for weak enough friction, the portion of the wave field that is far downstream of the mountain gives an overwhelmingly dominant contribution to the integral, whereas the contribution of the wave field near to the mountain, as well as the exact value of the lower limit of integration, are essentially irrelevant.

The integral in z in Equation (27) is calculated first. The result can be shown to be

$$\begin{aligned}
\int_z^{+\infty} U l_1^2 \zeta_{\mathrm{inv}}^2\, dz &= \frac{8\pi^2 U}{l_1^2 - l_2^2} \frac{|\hat{h}(k_L)|^2 m_1^2(k_L) n_2(k_L)}{k_L^2[1 + n_2(k_L)H]^2} \\
&\times \Bigg[l_2^2 m_1^2(k_L) + l_1^2(l_1^2 - l_2^2) n_2(k_L) \Bigg(H - z \\
&+ \frac{1}{2m_1(k_L)} \{\sin[2m_1(k_L)z] - \sin[2m_1(k_L)H]\} \Bigg) \Bigg] \\
&\times \sin^2(k_L x) \qquad \text{if } z < H, \\
\int_z^{+\infty} U l_2^2 \zeta_{\mathrm{inv}}^2\, dz &= \frac{8\pi^2 U l_2^2}{l_1^2 - l_2^2} \frac{|\hat{h}(k_L)|^2 m_1^4(k_L) n_2(k_L)}{k_L^2[1 + n_2(k_L)H]^2} \\
&\times \mathrm{e}^{-2n_2(k_L)(z-H)} \sin^2(k_L x) \qquad \text{if } z > H.
\end{aligned} \tag{29}$$

If Equation (29) is inserted into Equation (27), only the factors $\sin^2(k_L x)$ depend on x; hence, the following integral will arise:

$$\int_0^{+\infty} \sin^2(k_L x)\, \mathrm{e}^{-2k_I x}\, dx \approx \frac{1}{4k_I}, \tag{30}$$

where the approximation in Equation (30) becomes progressively more accurate as $k_I \to 0$. When this result is used, Equation (27) becomes

$$\begin{aligned}
\int_{-\infty}^{+\infty} uw\, dx &= -\frac{2\pi^2 \lambda U}{k_I(l_1^2 - l_2^2)} \frac{|\hat{h}(k_L)|^2 m_1^2(k_L) n_2(k_L)}{k_L^2[1 + n_2(k_L)H]^2} \\
&\times \Bigg[l_2^2 m_1^2(k_L) + l_1^2(l_1^2 - l_2^2) n_2(k_L) \Bigg(H - z \\
&+ \frac{1}{2m_1(k_L)} \{\sin[2m_1(k_L)z] - \sin[2m_1(k_L)H]\} \Bigg) \Bigg] \\
&\quad \text{if } z < H, \\
\int_{-\infty}^{+\infty} uw\, dx &= -\frac{2\pi^2 \lambda U l_2^2}{k_I(l_1^2 - l_2^2)} \frac{|\hat{h}(k_L)|^2 m_1^4(k_L) n_2(k_L)}{k_L^2[1 + n_2(k_L)H]^2} \\
&\times \mathrm{e}^{-2n_2(k_L)(z-H)} \qquad \text{if } z > H.
\end{aligned} \tag{31}$$

It remains to evaluate k_I. One might naively consider assuming that $k_I = \lambda/U$, given the form of the Rayleigh damping terms in Equations (6) and (7), but this is not correct. In order to obtain an accurate definition for k_I, it is necessary to go back to the wave solutions. In the inviscid trapped lee wave solution, the wavelength of the wave is determined by the (real) wave number at which the Fourier transform of the solution has a singularity. When friction is added to the problem, this singularity moves away from the real axis, corresponding to a complex value of the wave number at which the Fourier transform becomes infinite. The imaginary part of that wave number is k_I. The relevant wave solutions can be found in Teixeira *et al.* (2013a, Appendix A). For example, from their eq. (A1), it can be seen that the Fourier transform of the vertical velocity (which is proportional to the coefficient a_1) becomes singular (i.e., infinite) if the denominator of a_1 is zero; that is, if

$$m_1 \cos(m_1 H) - \mathrm{i} m_2 \sin(m_1 H) = 0. \tag{32}$$

In this equation, m_1, m_2, and the corresponding horizontal wave number k for which Equation (32) is satisfied may all be complex. To determine k_I, it must be noted that $m_1 = m_{1R} + \mathrm{i} m_{1I}$, $m_2 = m_{2R} + \mathrm{i} m_{2I}$ and $k = k_R + \mathrm{i} k_I$. This encompasses, for example, the cases in which m_2 is purely imaginary (in which case m_{2I} is named n_2—cf. Teixeira *et al.*, 2013a). In order for Equation (32) to be usable, it is necessary to express the sine and cosine functions in complex form and expand all the variables into their real and imaginary parts. Since the aim is to take friction into account, it is also necessary to assume definitions for m_1 and m_2 that are consistent with Equations (6)–(9). This is provided by eq. (12) of Teixeira *et al.* (2012), which is reproduced next:

$$m_j^2 = \frac{l_j^2}{1 - \mathrm{i}\frac{\lambda}{Uk}} - k^2, \tag{33}$$

where $j = 1, 2$, depending on whether it refers to the lower or upper layer respectively. The deceptively simple form of Equation (33), where the effect of friction is contained in λ, conceals the fact that both m_j and k are complex, yielding much lengthier expressions for the real and imaginary parts of this equation (of which an example, for real k, is provided by Teixeira *et al.* (2013a) (eqs. 14 and 15). To obtain k_I, both the real and imaginary parts of Equation (32) must be satisfied, which in a general case would produce equations that are too complicated. However, for weak friction, some simplifications are possible. For example, it is known that λ is small, but k_I is also expected to be small, since it is zero in the inviscid approximation. Additionally m_{1I} and m_{2R} are also expected to be small (they are also zero in the inviscid approximation). With these assumptions, only the leading order terms are not neglected in the equations for the real and imaginary parts of Equation (32). After a substantial amount of algebra, it turns out that, to leading order, Equation (32) reduces to

$$m_{1R} + m_{2I} \tan(m_{1R}H) = 0, \tag{34}$$

$$m_{1I}(1 + m_{2I}H) - (m_{2R} + m_{1R}m_{1I}H)\tan(m_{1R}H) = 0, \tag{35}$$

and Equation (33) can be expressed as

$$m_{jR}^2 = l_j^2 - k_R^2, \tag{36}$$

$$2m_{jR}m_{jI} = l_j^2 \frac{\lambda}{Uk_R} - 2k_R k_I, \tag{37}$$

where $j = 1, 2$ also apply to the lower or upper layer respectively. Note that Equations (34) and (36) define the wave resonance condition and the vertical wave number in the same way as in purely inviscid theory (with $m_{jR} = m_j$, $m_{2I} = n_2$, and $k_R = k$), whereas Equations (35) and (37) are equations where each term is of first order in the small quantities mentioned earlier. m_{1I} is small in the lower layer, whereas m_{2R} is small in the upper layer, and both λ and k_I are small in both layers. From Equations (34)–(37), it is possible to obtain k_I in terms of k_R. The final result is

$$k_I = \frac{\lambda}{2U}\frac{k_R^2 + l_1^2 n_2 H}{k_R^2(1 + n_2 H)}, \tag{38}$$

where $m_{2I} = n_2$ has been used. Noting that, for a flow with weak friction that satisfies Equation (32), $k_R = k_L$, and using Equation (38) with $n_2 = n_2(k_L)$ in Equation (31), the following expressions for the momentum flux are finally obtained:

$$\begin{aligned} M &= \rho_0 \int_{-\infty}^{+\infty} uw\, dx \\ &= -\frac{4\pi^2\rho_0 U^2}{l_1^2 - l_2^2} \frac{|\hat{h}(k_L)|^2 m_1^2(k_L) n_2(k_L)}{[1 + n_2(k_L)H][k_L^2 + l_1^2 n_2(k_L)H]} \\ &\quad \times \left[l_2^2 m_1^2(k_L) + l_1^2(l_1^2 - l_2^2)n_2(k_L)\left(H - z + \frac{1}{2m_1(k_L)}\{\sin[2m_1(k_L)z] - \sin[2m_1(k_L)H]\}\right)\right] \\ &\quad \text{if } z < H, \\ M &= \rho_0 \int_{-\infty}^{+\infty} uw\, dx \\ &= -\frac{4\pi^2\rho_0 U^2 l_2^2}{l_1^2 - l_2^2} \frac{|\hat{h}(k_L)|^2 m_1^4(k_L) n_2(k_L)\, \mathrm{e}^{-2n_2(k_L)(z-H)}}{[1 + n_2(k_L)H][k_L^2 + l_1^2 n_2(k_L)H]} \\ &\quad \text{if } z > H. \end{aligned} \tag{39}$$

From Equation (39), it can be concluded not only that the momentum flux is continuous at $z = H$ (as it should), but also that it reduces at the surface to minus the total pressure drag (confirming Equation (25)), namely:

$$M(z = 0) = -4\pi^2\rho_0 U^2 |\hat{h}(k_L)|^2 \frac{m_1^2(k_L) n_2(k_L)}{1 + n_2(k_L)H}, \tag{40}$$

which should be compared with Teixeira *et al.* (2013a, eq. 25). However, perhaps the most important feature of Equation (39) is that the momentum flux is independent of λ, because λ in the numerator of the fraction in Equation (31) cancels out with k_I—which is proportional to λ according to Equation (38)—in the denominator of the same fraction. This feature quantifies the intuitive qualitative result that was mentioned before when discussing Equation (23), about the inverse variation of the spatial extent of the trapped lee wave train with λ.

Equation (39) is the main result of the present section. It gives a closed-form expression (except for the necessarily numerical root-finding procedure to determine k_L) for the momentum flux associated with trapped lee waves in the two-layer atmosphere of Scorer (1949). It probably represents the closest one can get to an inviscid solution for the momentum flux produced by trapped lee waves for that model atmosphere; but, as we saw, the inclusion of friction (no matter how weak), is essential to obtain it consistently. Hereafter, Equation (39) will be called the quasi-inviscid theory or solution. For comparison, the purely inviscid solution for M (with an upper limit of integration x replacing $+\infty$) from Broad (2002)—deriving from the first term on the right-hand side of Equation (14), involving w^2—takes the following form, for the two-layer atmosphere of Scorer (1949):

$$\begin{aligned} M_B &= -\frac{4\pi^2\rho_0 U^2}{l_1^2 - l_2^2} \frac{|\hat{h}(k_L)|^2 m_1^2(k_L) n_2(k_L)}{[1 + n_2(k_L)H]^2} \\ &\quad \times \left[m_1^2(k_L) + (l_1^2 - l_2^2)n_2(k_L)\left(H - z + \frac{1}{2m_1(k_L)}\{\sin[2m_1(k_L)z] - \sin[2m_1(k_L)H]\}\right)\right] \\ &\quad \times \cos^2(k_L x) \qquad \text{if } z < H, \\ M_B &= -\frac{4\pi^2\rho_0 U^2}{l_1^2 - l_2^2} \frac{|\hat{h}(k_L)|^2 m_1^4(k_L) n_2(k_L)\, \mathrm{e}^{-2n_2(k_L)(z-H)}}{[1 + n_2(k_L)H]^2} \\ &\quad \times \cos^2(k_L x) \qquad \text{if } z > H. \end{aligned} \tag{41}$$

The momentum flux deriving from the second and third terms on the right-hand side of Equation (14) (involving u^2 and ζ^2), on the other hand, may be written

$$M_{NB} = -\frac{4\pi^2\rho_0 U^2}{l_1^2 - l_2^2} \frac{|\hat{h}(k_L)|^2 m_1^2(k_L) n_2(k_L)}{k_L^2[1 + n_2(k_L)H]^2}$$

$$\times\left(m_1^2(k_L)[l_2^2-n_2^2(k_L)]+k_L^2(l_1^2-l_2^2)n_2(k_L)(H-z)\right.$$
$$+\frac{[l_1^2+m_1^2(k_L)](l_1^2-l_2^2)n_2(k_L)}{2m_1(k_L)}$$
$$\left.\times\{\sin[2m_1(k_L)z]-\sin[2m_1(k_L)H]\}\right)\sin^2(k_Lx)$$
$$\text{if } z<H,$$
$$M_{NB}=-\frac{4\pi^2\rho_0U^2}{l_1^2-l_2^2}$$
$$\times\frac{|\hat{h}(k_L)|^2m_1^4(k_L)n_2(k_L)[l_2^2-n_2^2(k_L)]\,e^{-2n_2(k_L)(z-H)}}{k_L^2[1+n_2(k_L)H]^2}$$
$$\times\sin^2(k_Lx)\qquad \text{if } z>H. \tag{42}$$

The total inviscid solution is the sum of Equations (41) and (42), M_B+M_{NB}. Note that, unlike in Equation (39), M_B and M_{NB} depend on the upper limit of integration x via the phase of the (infinite) trapped lee wave (the $\cos^2(k_Lx)$ and $\sin^2(k_Lx)$ factors included in these expressions). Additionally, M_B and M_{NB} are in quadrature. So, when $\sin(k_Lx)=0$—the situation envisaged by Broad (2002)—$M_{NB}=0$ and M_B is a maximum, whereas $M_B=0$ and M_{NB} is a maximum when $\cos(k_Lx)=0$. The form of the variation with height of M_{NB} is, however, very different from that of M_B—or of M as given by Equation (39)—as will be seen next.

3 | NUMERICAL MODELS

To compare and validate the previous results from linear theory, two models will be used. One of them is a linear model that includes friction exactly in the same form as envisaged in the theory described earlier herein, but where the Rayleigh damping coefficient may take an arbitrary value. The second model is a numerical model where the fully nonlinear dynamics of the waves can be represented. These are described next in turn.

3.1 | Linear model with friction

This linear model departs from exactly the same equation set as used in the preceding calculations, comprising Equations (6)–(9). The approach is similar to that adopted in Teixeira *et al.* (2012). Since friction is always non-zero, and hence the flow perturbations associated with the trapped lee waves always decay downstream (i.e., they are bounded spatially), these perturbations can be expressed as Fourier integrals. The Fourier transform of the vertical velocity $\hat{w}$ (in terms of which all other flow perturbation variables may be expressed) satisfies eq. (6) of Teixeira *et al.* (2012). The vertical wave number of the waves m (which for the two-layer atmosphere of Scorer takes different values in the lower and upper layer) may be expressed as in eq. (12) of Teixeira *et al.* (2012) (with l_0 replaced by l_1 in the lower layer and by l_2 in the upper layer). This wave number is, of course, complex, with real and imaginary parts m_R and m_I given by eqs 14 and 15 of Teixeira *et al.* (2012) (again with l_0 replaced by l_1 or l_2). The procedure to obtain m_R and m_I is entirely analogous to that described in Teixeira *et al.* (2012), with the difference that boundary conditions for $\hat{w}$ and $d\hat{w}/dz$ (resulting from continuity of pressure) must be satisfied at $z=H$, in the same way as was necessary for the derivation of Equation (28).

From Equation (5), which in this case is valid because w is bounded spatially, and from mass conservation, Equation (9), expressed in terms of Fourier transforms, it can be shown that the momentum flux is given by

$$M=4\pi\rho_0\times\int_0^{+\infty}\left\{\mathrm{Im}(\hat{w})\frac{\partial}{\partial z}[\mathrm{Re}(\hat{w})]-\mathrm{Re}(\hat{w})\frac{\partial}{\partial z}[\mathrm{Im}(\hat{w})]\right\}\frac{dk}{k}, \tag{43}$$

where the fact that the integrand is symmetric with respect to k has been taken into account. The integral in Equation (43) is not analytical in the presence of friction (i.e., with $\lambda>0$) and so must be calculated numerically, using a Gauss–Legendre quadrature algorithm. In this calculation, λ cannot be too low, otherwise the contribution to the integral concentrates progressively more around a singularity (corresponding to the inviscid resonant trapped lee wave mode), and the numerical integration procedure fails. In practice, and as will be seen, a friction coefficient as small as necessary to make the results converge to those of the quasi-inviscid theory (presented previously) can be used.

3.2 | Nonlinear numerical model

Numerical simulations are carried out using the micro-to-mesoscale model FLEX (Argaín, 2003; Argaín *et al.*, 2009; 2017). This is a 2D fully nonlinear and time-dependent numerical model using curvilinear orthogonal coordinates with grid refinement near the ground, which is able to accurately represent boundary-layer flows. Here, the model is run in inviscid mode, since the primary aim is to test the theoretical results presented earlier herein before any additional flow complications are considered.

The domain of integration consists of 556 grid points in the horizontal direction and 2,244 grid points in the vertical. With a grid spacing of 180 m in the horizontal and 7 m in the vertical, this yields a domain size of 100 km in the horizontal and 15.7 km in the vertical. The time step of the simulations is 0.5 s. In all experiments, the orography corresponds to a 2D bell-shaped mountain, with terrain elevation given by

$$h(x) = \frac{h_0}{1 + (x/a)^2}, \tag{44}$$

where the mountain half-width is $a = 1$ km and the mountain height is $h_0 = 10$ m. The wind speed is constant (the lower boundary condition is free-slip) with a magnitude $U = 10\,\mathrm{m{\cdot}s^{-1}}$, and the Brunt–Väisälä frequency in the lower layer is $N_1 = 0.02\,\mathrm{s^{-1}}$, yielding a Scorer parameter of $l_1 = N_1/U = 2 \times 10^{-3}\,\mathrm{m^{-1}}$. The Brunt–Väisälä frequency in the upper layer is defined by the assumed ratio $N_2/N_1 = l_2/l_1$, which varies between simulations. The flow regime is strongly linear ($l_1 h_0 = 0.02$) and strongly non-hydrostatic ($l_1 a = 2$), which favours the existence of trapped lee waves that can dominate the flow (Teixeira *et al.*, 2013a). Given the aforementioned parameters, the horizontal domain length corresponds to $100a$, with $10a$ extending upstream of the mountain and $90a$ extending downstream. The purpose of this asymmetry is to focus on the trapped lee waves, which only exist downstream of the orography and can persist for a long distance, especially in inviscid numerical simulations. The vertical domain length corresponds to five vertical wavelengths of the hydrostatic mountain waves for the parameters of the lower layer, $\lambda_1 = 2\pi U/N_1 = 2\pi/l_1 \approx 3.1$ km. Trapped lee wave modes with (horizontal) wavelengths between ≈4.5 km and ≈11 km are generated, values that can be confirmed to a good degree of accuracy using linear theory from the assumed flow parameters—more details about the wave modes and wavelength behaviour for similar flow conditions can be found in Teixeira *et al.* (2013a). Sponge layers with thickness $4a$ exist at the upstream and downstream boundaries of the domain. A sponge layer with thickness $2\lambda_1 \approx 6.3$ km exists at the top of the domain.

The simulations are run until a time when an approximate steady state is reached by the wave momentum flux profile. This time can vary approximately between $100a/U \approx 2.8$ hr and $400a/U \approx 11.1$ hr.

4 | PRELIMINARY RESULTS

Preliminary tests of the theory developed in Section 2 will be divided into two parts. First, comparisons will be made with perfectly inviscid solutions, of the same type as those produced by Broad (2002) and included in the treatment presented earlier herein. Second, the quasi-inviscid solutions (with vanishing but non-zero friction), which constitute the bulk of the preceding theoretical treatment and are those of greatest practical importance, will be tested.

Before this is done, it is useful to check whether the theory, linear model with friction, and numerical simulations are comparable. Figure 2 shows the normalized vertical and horizontal flow perturbations associated with the waves generated for flow of the two-layer atmosphere of Scorer over a very small amplitude bell-shaped mountain, described by Equation (44). The dimensionless input parameters on which the normalized results of the linear theory depend are l_2/l_1, $l_1 H/\pi$, and $l_1 a$ (Teixeira *et al.*, 2013a), which are expected to be the same as for the inviscid simulations of the FLEX model (since $l_1 h_0 = 0.02$ is very small). It is assumed that $l_2/l_1 = 0.2$, $l_1 a = 2$, and $l_1 H/\pi = 0.6$. An additional input parameter in the linear model with friction is $\lambda U/a$. As can be seen, the behaviour of the three models for $x > 0$ is very similar, with trapped lee waves totally dominating the flow—compare with fig. 18b of Teixeira *et al.* (2013a) for $l_1 H/\pi = 0.8$ instead. The wavelength of the waves, and even the intensity of their velocity perturbations (evaluated by the number of contours), is quite similar between all cases, with the difference that the wave from inviscid linear theory is perfectly monochromatic and so must be disregarded for $x < 0$. The linear model with friction correctly suppresses the wave upstream of the mountain, albeit showing some differences in structure relative to the FLEX numerical simulation.

The most important message conveyed by Figure 2, however, is that the structure of the trapped lee wave is, for x somewhat larger than zero (say, $x/a > 5$), almost indistinguishable between the three models. This corroborates the assumption underlying the calculations presented earlier herein that, for vanishing friction, it is appropriate to redefine the lower limit of integration in Equation (23) as zero. This is because an overwhelming contribution to the integral comes from substantially larger x, where the approximation from inviscid linear theory is very accurate, so the exact value of this lower integration limit and the behaviour of the wave solution in its vicinity are irrelevant. This result ultimately relies on the asymptotic approximation of Scorer (1949), but its relevance for the specific purpose of evaluating the integral in Equation (23) should be emphasized here.

4.1 | Inviscid results

The extension of the results of Broad (2002) presented in Section 2 will now be tested against numerical simulations. For this purpose, the inviscid linear model is compared with inviscid FLEX runs. Since, according to Section 2, the horizontal flux of vertical momentum, defined with a $+\infty$ upper limit of integration, does not converge for purely inviscid flow, the definition using x instead as upper

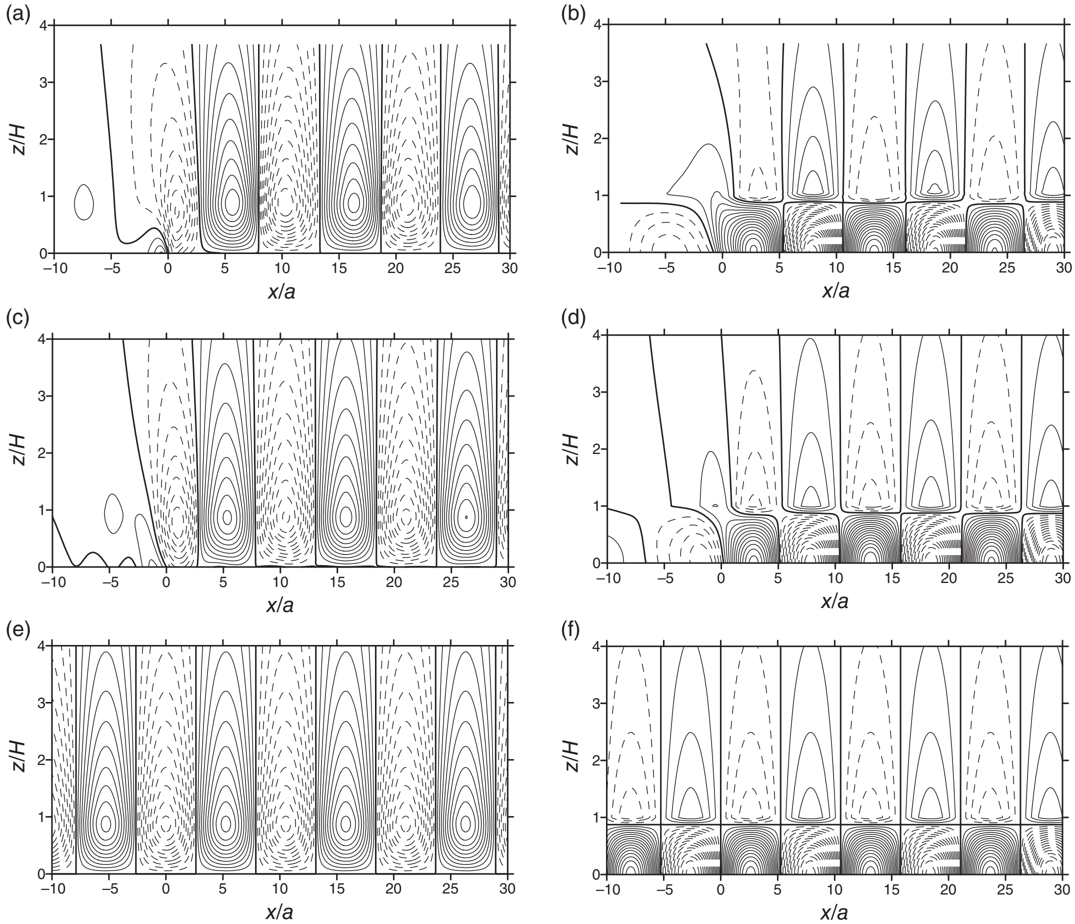

FIGURE 2 (a, c, e) Normalized vertical velocity perturbation $w/(Uh_0/a)$ and (b, d, f) normalized horizontal velocity perturbation $u/(N_1h_0)$ for the two-layer atmosphere of Scorer, for $l_2/l_1 = 0.2$, $l_1H/\pi = 0.6$, and $l_1a = 2$, from (a, b) FLEX numerical simulations, (c, d) linear model with friction for $\lambda a/U = 5 \times 10^{-4}$, and (e, f) inviscid linear theory. Note that the results from linear theory in (e, f) should be disregarded for $x < 0$. Contour spacing: 0.2; solid contours: positive values; dashed contours: negative values

limit of integration, included in Equation (18), is adopted here.

Figure 3 shows this momentum flux (corresponding to $M_{\rm B} + M_{\rm NB}$ defined according to Equations (41) and (42), but here also denoted by M, for convenience), normalized by the surface drag produced by hydrostatic waves in an atmosphere similar to the lower layer, but extending indefinitely, $D_0 = (\pi/4)\rho_0U^2l_1h_0^2$ (Teixeira *et al.*, 2013a), in three different ways. Figure 3a shows the momentum flux as a function of downstream distance at three different heights: $z/H = 0$, 0.5, and 1. M/D_0 oscillates with downstream distance (with an especially high amplitude at $z/H = 0.5$) except at $z = 0$. This latter result highlights the well-posedness of the inviscid surface drag problem, which Teixeira *et al.* (2013a) took advantage of. It is due to the fact that $z = 0$ is the only height at which the trapped lee waves do not extend indefinitely, because of the surface boundary condition. Since the product of u and w is rather sensitive to phase differences in the oscillations, in addition to fluctuations in magnitude, the field of $-M/D_0$ from FLEX (solid lines) is not as regular in Figure 3a as those of w and u in Figure 2, showing some modulation, part of which, existing in the left two-thirds of the domain, has unclear causes. Nance and Durran (1998) noted a similar effect previously, even for mountains of very low amplitude (see their fig. 1a). The monotonic amplitude decay existing towards the right edge of the domain is due to the effect of the lateral sponge at the downstream boundary, but this effect appears to extend considerably beyond the space occupied by the sponge itself. Naturally, any amplitude modulation is totally absent in the results from inviscid linear theory (dashed lines). However, the overall magnitude of $-M/D_0$, the amplitude of its oscillations, their wavelength (which is half the wavelength of the trapped lee waves), and phase are in quite good agreement with the numerical simulations, particularly for $k_{\rm L}x/\pi < 11$. This suggests averaging these fields over a number of wave cycles to make the comparison easier.

Figure 3b shows such an average, for the same heights as considered in Figure 3a, taken over the wave cycles

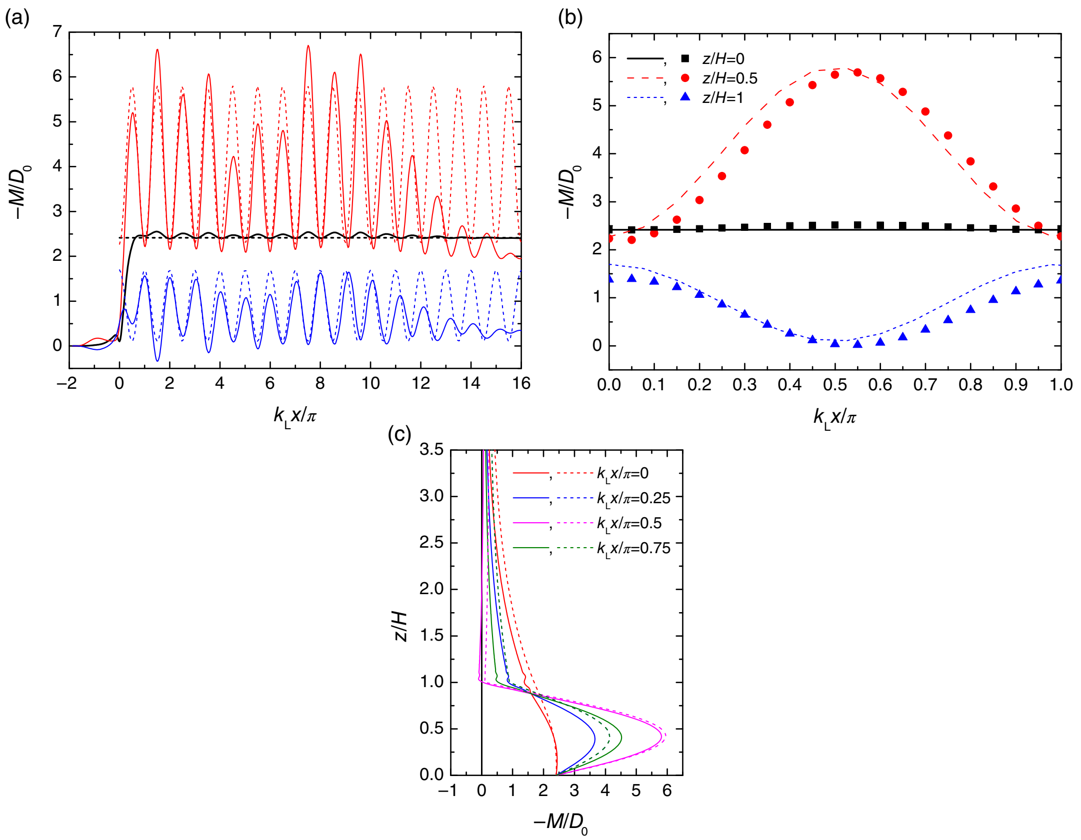

FIGURE 3 (a) Normalized momentum flux at three different levels from the FLEX model (solid lines) and from inviscid linear theory (Equations 41 and 42) (dashed lines), for the two-layer atmosphere of Scorer with $l_2/l_1 = 0.2$, $l_1H/\pi = 0.6$, and $l_1a = 2$. The horizontal coordinate is normalized using the theoretical wave number of the trapped lee waves, k_L. Black lines: $z/H = 0$, red lines: $z/H = 0.5$, blue lines: $z/H = 1$. (b) Normalized momentum flux as a function of the wave phase, averaged over $1 < k_Lx/\pi < 10$ from (a). Symbols: FLEX model; lines: inviscid linear model (see legend for details). (c) Profiles of the normalized momentum flux for key values of the wave phase (averaged as in panel b). Solid lines: FLEX model; dashed lines: inviscid linear theory. See legend for details (note that the dashed blue line coincides with the dashed green line and is hidden by it) [Colour figure can be viewed at wileyonlinelibrary.com]

existing between $k_Lx/\pi = 1$ and 10. The lower limit of k_Lx/π is dictated by the fact that the oscillation is not yet quasi-periodic for $0 < k_Lx/\pi < 1$ and the upper limit by the decay of the oscillation towards the downstream boundary of the domain. It can be seen that the magnitude of $-M/D_0$, as well as the amplitude and phase of its oscillation over a wave cycle is in good agreement between FLEX and inviscid linear theory. The amplitude of the oscillation is a bit smaller in FLEX than in linear theory at $z/H = 1$, and the oscillation is slightly out of phase at both $z/H = 0.5$ and 1 owing to the slightly larger wavelength of the trapped lee waves in the numerical simulations (see Figure 3a).

In Figure 3c, full profiles of $-M/D_0$ are presented for key values of the wave phase. $k_Lx/\pi = 0$ is the point at which both the u and ζ flow perturbations are zero and w is a maximum—that is, the reference point considered by Broad (2002). At $k_Lx/\pi = 0.5$, $-M/D_0$ is in phase opposition to the preceding case, with the u and ζ velocity perturbations being at their maxima and w being zero. The intermediate phase points correspond to $k_Lx/\pi = 0.25$ and 0.75. Clearly, the most interesting results are for $k_Lx/\pi = 0$ and 0.5, as $-M/D_0$ behaves in an intermediate way for $k_Lx/\pi = 0.25$ and 0.75. When $k_Lx/\pi = 0$—corresponding to the original calculations of Broad (2002)—$dM/dz = 0$ at $z = 0$ (a feature, that, as will be seen, is preserved in the quasi-inviscid results with vanishing friction), and dM/dz is continuous at $z = H$. These "desirable" features (which result directly from the fact that w^2 is zero at $z = 0$ and continuous at $z = H$) may have influenced Broad (2002) to privilege this particular result. On the other hand, for $k_Lx/\pi = 0.5$, $-dM/dz$ is positive at $z = 0$, with $-M/D_0$ attaining a maximum slightly below $z/H = 0.5$ that is more than twice its value at $z = 0$, and dM/dz is discontinuous at $z = H$, with very small values of $-M/D_0$ in the upper layer. This is due to the fact that u^2, which is non-zero at $z = 0$ and discontinuous at $z = H$, contributes in this case to $-dM/dz$. Agreement between the FLEX model and linear theory is good, especially considering the very large modulation that $-M/D_0$ undergoes over the wave cycle, but $-M/D_0$ from FLEX is slightly lower than from linear theory in the upper layer. There is a difference in the profiles of $-M/D_0$ at $k_L x/\pi = 0.25$ and 0.75 from FLEX, which does not exist in those from linear theory, because of the phase difference between the two oscillations, shown in Figure 3b and commented on earlier herein.

Overall, it can be concluded that the FLEX model, run in inviscid mode, reproduces the main physical aspects of the structure of the momentum flux predicted by the inviscid linear theory presented before, which extends the analysis of Broad (2002). The results emphasize that the vertical flux of horizontal momentum does not, in this case, take a unique form.

4.2 | Results with vanishing friction

Comparisons of inviscid simulations of the FLEX model with the quasi-inviscid linear theory (including vanishingly small friction) are presented next. First of all, it is necessary to ascertain that this linear theory does, indeed, accurately represent the limit of very small, but non-zero, friction. This is done in Figure 4a, which shows profiles of the normalized momentum flux from the quasi-inviscid linear theory (black line) and from the linear model with finite friction (colour lines), for $l_2/l_1 = 0.2$, $l_1 H/\pi = 0.6$, and $l_1 a = 2$ (the same conditions as considered in Figures 2 and 3). In these results, the definition of M includes the upper limit of integration $+\infty$, as is consistent with any non-zero friction (since the trapped lee waves necessarily decay downstream, no matter how slowly).

In Figure 4a, the momentum flux profiles are clearly very different from any of those presented in Figure 3c, including that from Broad (2002). For sufficiently weak friction, $dM/dz = 0$ at $z = 0$, but dM/dz is discontinuous at $z = H$, with $-M/D_0$ being much smaller in the upper layer than in the lower layer. Both aspects can be explained by differentiating Equation (23) with respect to z, yielding

$$\frac{\partial}{\partial z}\int_{-\infty}^{+\infty} uw\, dx = \frac{\lambda}{U}\left(N^2 - U\frac{d^2U}{dz^2}\right)\int_{-\infty}^{+\infty} \zeta^2\, dx. \quad (45)$$

If this equation is applied at $z = 0$, it reduces to

$$\left(\frac{\partial}{\partial z}\int_{-\infty}^{+\infty} uw\, dx\right)(z=0) = \frac{\lambda}{U(z=0)} \times \left[N^2(z=0) - U(z=0)\frac{d^2U}{dz^2}(z=0)\right]\int_{-\infty}^{+\infty} h^2\, dx, \quad (46)$$

where $\zeta(z=0) = h$ has been used. Since $h(x)$ does not depend on λ, the right-hand side of Equation (46) approaches zero as $\lambda \to 0$ (note that this does not occur for $z > 0$, because ζ^2 then extends downstream for a distance proportional to U/λ). When $z > 0$, Equation (45) shows that dM/dz is proportional to N^2 (if $d^2U/dz^2 = 0$), and that is why in Figure 4a there is a discontinuity in dM/dz at $z = H$, where N is discontinuous. This is, however, a specific feature of Scorer's two-layer atmosphere and would not exist for a more realistic static stability profile.

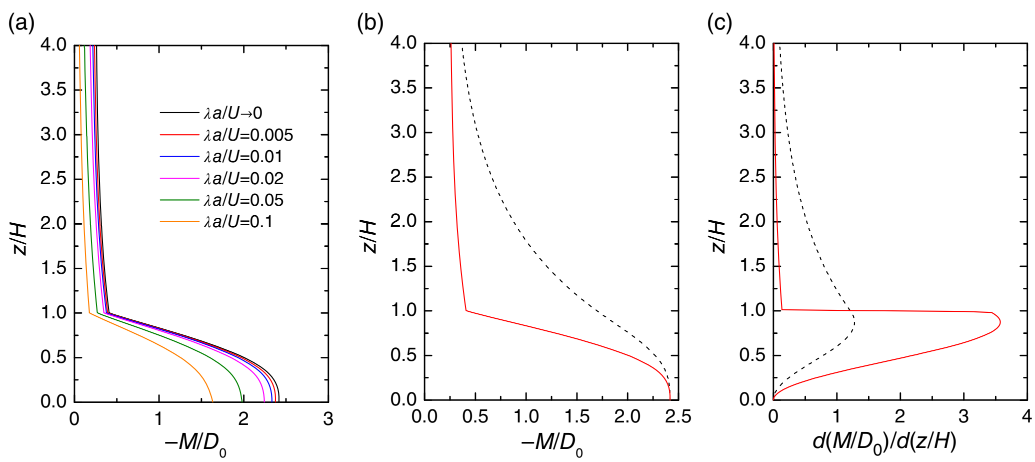

FIGURE 4 (a) Normalized momentum flux profiles from quasi-inviscid linear theory (black line, corresponding to Equation (39)) and from the linear model with friction (according to Equation (43)), for the two-layer atmosphere of Scorer with $l_2/l_1 = 0.2$, $l_1 H/\pi = 0.6$ and $l_1 a = 2$, for different values of the friction coefficient $\lambda a/U$ (see legend for details). (b) Momentum flux and (c) momentum flux divergence profiles, for the same input parameters, from Broad's theory, Equation (41) (black dashed line), and from quasi-inviscid theory, Equation (39) (red solid line). [Colour figure can be viewed at wileyonlinelibrary.com]

Figure 4a shows that the model with friction seamlessly approaches the quasi-inviscid theory as $\lambda a/U$ decreases to zero. In particular, it can be seen that, in order for the $-M/D_0$ profile to be distinguishable between the two models, it is necessary that $\lambda a/U$ is substantially larger than the value assumed in Figure 2c,d. This corroborates that the quasi-inviscid linear theory is a consistent limit of the problem with friction as $\lambda \to 0$, with the advantage that it provides closed analytical expressions for the momentum flux (for this simplified atmosphere). A final aspect to note is that the non-zero value to which $-M/D_0$ asymptotes in the upper layer is due to the propagation of non-trapped waves, which are associated with a constant momentum flux profile (in the absence of any critical levels, as is the case). This non-zero constant is, however, by deliberate choice of the input parameters, a relatively small fraction of the total momentum flux, as this allows focusing primarily on the trapped lee waves. For reasons explained in Teixeira *et al.* (2013a), these two components of the momentum flux (like the corresponding components of the surface drag) may be simply added.

Figure 4b,c exemplifies how the results from quasi-inviscid theory, Equation (39), differ from those predicted by Broad's theory, Equation (41), for the same conditions as considered in Figure 4a. Although in Figure 4b the two results for $-M/D_0$ coincide at the surface and at high levels, they differ most in the region centred around $Z/H = 1$, where Broad's model overestimates quasi-inviscid theory considerably. More importantly for drag parametrization, the divergence of the momentum flux shown in Figure 4c predicted by quasi-inviscid theory exceeds by a factor >3 that predicted by Broad's theory immediately below the interface separating the two layers, and is smaller by an even larger factor in the upper layer. Admittedly, this is a rather extreme example of this discrepancy, and the discontinuity in $d(M/D_0)/d(z/H)$ displayed by quasi-inviscid theory is, as pointed out earlier, an artefact of Scorer's two-layer atmosphere.

In Figure 5, a comparison is made of a limited subset of momentum flux profiles for the two-layer atmosphere of Scorer, between the FLEX model and the quasi-inviscid linear theory. To reproduce the conditions envisaged in theory as closely as possible, in FLEX the momentum fluxes are integrated horizontally over the full length of the computational domain, including the sponge damping layers. Despite considering a range of values of l_2/l_1 and l_1H/π, the results presented in Figure 5 (like all the preceding results) are focused exclusively on the first trapped lee wave mode among the possible modes supported by Scorer's atmosphere—as can be checked against fig. 1 of Teixeira *et al.* (2013a) from the values of l_2/l_1 and l_1H/π assumed here. This choice is made because the first trapped lee wave mode is the strongest one and that likely to be represented most accurately in numerical simulations (as the wave reflection occurs closer to the ground, leading to less dispersive weakening of the waves), and also because the absence of additional wave modes makes the problem as "clean" as possible to illustrate the quasi-inviscid theory developed here. Of course, the theory is applicable to a much wider range of conditions. For $l_2/l_1 = 0.6$, the lowest value of l_1H/π is 0.7 instead of 0.6, because $l_1H/\pi = 0.6$ is theoretically expected to have zero trapped lee waves modes (by a narrow margin), and the focus here is on trapped lee waves. Values of l_1H/π adopted in Figure 5 are also concentrated within the lower half of the interval spanned by l_1H/π corresponding to a single wave mode, because, as shown by Teixeira *et al.* (2013a), the wavelength (Teixeira *et al.*, 2013a, fig. 6b) and the trapped lee wave amplitude (inferred from the corresponding drag; Teixeira *et al.*, 2013a, fig. 6d,e), as well as the relative magnitude of the trapped lee wave drag compared with the drag of waves that propagate vertically into the upper layer, are all maximized for these conditions.

Figure 5 confirms the results of quasi-inviscid theory with good accuracy, with a few exceptions in detail. Overall, both the surface value and shape of the profiles of $-M/D_0$ from FLEX and from the quasi-inviscid theory are in good agreement. Even in the cases where agreement is not perfect (surface value of $-M/D_0$ in Figure 5a–e, values of $-M/D_0$ in the upper layer in Figure 5c,d,f), the fractional difference is typically small, and qualitative agreement is very good. In particular, the results from FLEX confirm the zero value of dM/dz at the surface and its discontinuity at $z = H$ (where the momentum flux from FLEX displays some oscillations, presumably of numerical origin). This discontinuity obviously becomes weaker as l_2/l_1 increases, because dM/dz was seen in Equation (45) to be proportional to N^2. It is noteworthy that the magnitude of $-M/D_0$ at $z = 0$ (which corresponds to the total surface drag) decreases both as l_2/l_1 and l_1H/π increase. The first result is due to the fact that the intensity of the wave reflection that generates the resonant trapped lee waves is proportional to the contrast in static stability between the two layers. The second result is due to the fact that, for a given mode, the intensity of the trapped lee waves (of which the associated drag is a good measure) decreases as l_1H/π increases—this was first noted by Corby and Wallington (1956), and can be confirmed in Teixeira *et al.* (2013a, fig. 6d). As noted earlier herein, this occurs due to dispersion effects. The momentum flux associated with waves that propagate vertically in the upper layer (shown by $-M/D_0$ near the top of the domain displayed in Figure 5) has constant magnitude with height (as there are no critical levels), and in the quasi-inviscid theory was simply added to the momentum flux associated with trapped lee waves, since it comes from

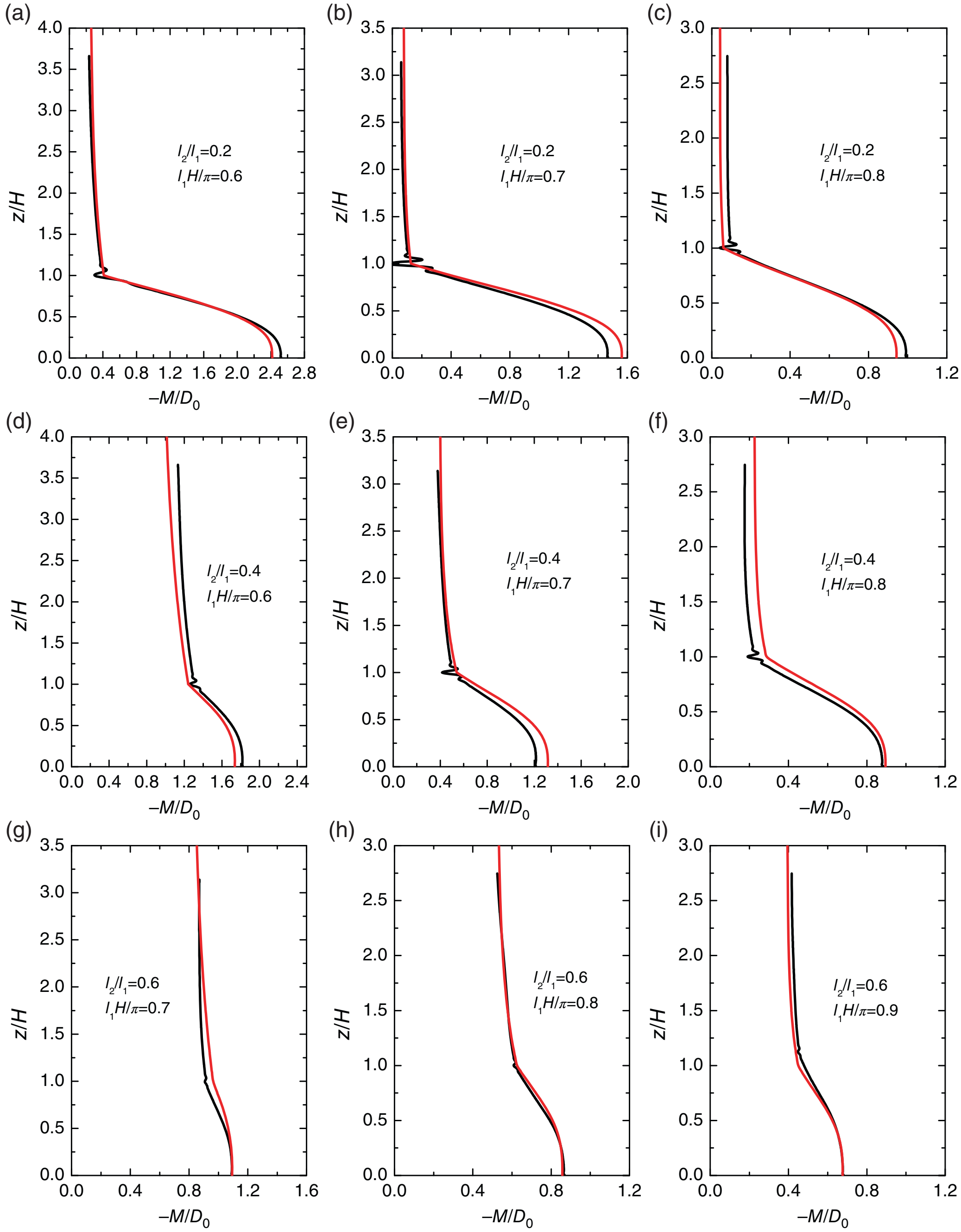

FIGURE 5 Normalized momentum flux profiles for the two-layer atmosphere of Scorer for $l_1a = 2$ and different values of l_2/l_1 and l_1H/π (see legends for details). Black lines: FLEX model; red lines: quasi-inviscid linear theory, Equation (39) [Colour figure can be viewed at wileyonlinelibrary.com]

a lower, independent range of wave numbers. A similar result was obtained for the surface drag by Teixeira *et al.* (2013a). The part of the momentum flux associated with vertically propagating waves does not behave monotonically with the input parameters. It clearly decreases when l_1H/π increases, but its variation with l_2/l_1 is not as obvious. However, it can be noticed that, in relative terms, the momentum flux associated with vertically propagating waves becomes more important compared with that associated with trapped lee waves as l_2/l_1 increases, since the former waves do not require reflection at a layer to exist, unlike the latter. Vertically propagating waves are also (partially) reflected at $z = H$, but this does not make their momentum flux vary between the two layers, in accordance with the traditional form of the Eliassen–Palm theorem.

One aspect deserving a more detailed analysis is that whereas in quasi-inviscid theory the decay of the trapped lee waves with distance downstream—which enabled the calculation of the momentum flux from Equation (39)—is exponential (see Equation (26)), in the FLEX numerical model it takes quite a different form. Although the wave field, and especially the partially integrated momentum flux, is rather noisy (as shown in Figure 3), in the part of the computational domain outside the lateral sponges the FLEX model is nominally inviscid, so the amplitude of the trapped lee wave should be roughly constant. When the downstream lateral sponge is reached, the wave field decays to zero in some way prescribed by the sponge damping. Since Equation (39) was derived assuming an exponential decay, the fact that the FLEX results are so close to those of the quasi-inviscid theory is puzzling. The explanation may be in the more general form of the momentum flux expressed by Equation (27). In that equation, clearly, if the factor modulating the amplitude along x (an exponential in this case, but it could be any other function that decays to zero as $x \to +\infty$) does not depend on z, the shape of the profile of M is determined only by the integral in the z direction. The integral in the x direction just plays the role of limiting the magnitude of the term on the right-hand side of Equation (27), being therefore equivalent to a scaling factor. It can thus be argued that, for any type of downstream decay of the trapped lee wave caused by weak friction that does not depend on z, the result produced by Equation (27) still holds. This endows the present results with considerable generality, making them more relevant. The results also suggest that dissipation in the sponge layer existing at the downstream boundary of the domain in the FLEX simulations can be considered weak (as this is one of the assumptions in quasi-inviscid theory). This is consistent with the requirement that wave decay in the sponge layer be sufficiently gradual to avoid upstream reflections. It also seems likely that the assumption of weak dissipation is satisfied often in nature, as suggested by the considerable spatial extent of many observed trapped lee wave patterns.

5 | CONCLUSIONS

This study presents a long overdue new theory for the momentum fluxes associated with trapped lee waves, whose divergence corresponds to the drag exerted by mountains on the atmosphere, mediated by the waves. As a first approximation, linear 2D trapped lee waves were considered, to build the necessary theoretical framework under the most basic assumptions. Friction, which needs to be taken into account, was included in the simplest possible form, as a Rayleigh damping applied only to the momentum equations. The calculations were developed in the limit of vanishing friction (a Rayleigh damping coefficient λ approaching zero). The solutions to the trapped lee waves and associated wave momentum flux problem were found to be self-consistent in this limit, providing a simplified framework that allows maximally general analytical results to be obtained.

The wave momentum flux was found to be expressed in terms of the product of λ and an integral in space (in the horizontal and vertical directions) involving a quadratic quantity of the wave field: the square of the vertical streamline displacement. This integral increases in inverse proportion to λ (because as λ decreases the waves extend for a larger distance before they decay). So, despite the fact that the momentum flux is written in terms of an expression involving λ, this dependence cancels out in the limit $\lambda \to 0$, yielding a quasi-inviscid approximation that is well-posed mathematically, finite, and independent of λ. Although the details of this result rely on the adopted Rayleigh damping formulation for friction, the underlying logic extends to other forms of friction. It is plausible, for example, that the same arguments would qualitatively apply to momentum fluxes calculated with the diffusive representation of friction adopted by Soufflet *et al.* (2022).

The results were illustrated by application to the two-layer atmosphere of Scorer, where wave trapping is induced by a piecewise constant profile of static stability, with a discontinuity at the top of the trapping layer. For this atmosphere, the results mentioned earlier herein about the independence of the momentum flux profile from λ in the limit $\lambda \to 0$ were explicitly confirmed. It was possible to derive a closed-form analytical expression for the momentum flux profile, which is different from any of the expressions for the partial momentum flux (i.e., only extending up to a certain part of the trapped lee wave train downstream of the mountain) that could be obtained by extension of the perfectly inviscid theory of Broad (2002). As a general result, and for quasi-inviscid conditions, the momentum flux divergence is zero at the ground, as originally predicted by Broad (2002), although, of course, boundary-layer effects (which might be addressed in a future study) are likely to modify the behaviour of the momentum flux near the surface (Turner *et al.*, 2021). Specifically for Scorer's atmosphere, there is a discontinuity in the momentum flux divergence at the interface between the two layers, since that divergence is proportional to the static stability N^2. This yields momentum flux divergence profiles that are quite different from those predicted by Broad's theory (which are continuous at this interface), corresponding to a larger drag exerted on the atmosphere near the top of the lower layer, and much lower drag within the upper layer. For Scorer's atmosphere, the momentum flux associated with waves that propagate vertically into the upper layer has no divergence, but its magnitude varies according to the relative importance of those waves and trapped lee waves. In the present study, cases where trapped lee waves are dominant have been selected, since these are totally responsible for the momentum flux divergence at low levels. One aspect on which the present quasi-inviscid theory and that of Broad (2002) agree is the magnitude of the momentum flux at $z = 0$ (which coincides with the total surface drag for weak friction). This is a consequence of the fact that the problem of trapped lee wave surface drag is well-posed mathematically, even for perfectly inviscid flow (Teixeira *et al.*, 2013a; 2013b). This is because contributions to this drag are confined to the vicinity of the isolated orography generating the trapped lee waves, even if the waves themselves extend indefinitely downstream.

The present preliminary results should be viewed as a useful contribution to the establishment of a workable theory of the momentum fluxes produced by trapped lee waves and their impact on the atmosphere. However, what the theory, as described in this study, provides is only the vertical flux of horizontal momentum integrated over the total area (in this 2D case, distance) spanned by the waves. Since trapped lee waves can extend over quite a large area (or long distance) downstream of their source, to know their integrated effect as a function of height (which is what is provided here) is highly relevant but not the whole story. It would also be useful to obtain the local impact of the trapped lee waves on the mean flow at given points within the wave field, as that region is likely to occupy a substantial range of model grid-points in reasonably high-resolution weather prediction numerical simulations. A treatment of this aspect would require knowing not only the vertical flux of horizontal momentum at each point (or at least over a smaller finite area), but also the horizontal flux of horizontal momentum (since, in the middle of the trapped lee wave field, the latter is not zero). Xue and co-workers (Xue and Giorgietta, 2021; Xue *et al.*, 2022), for example, attempted to interpret their numerical simulations of trapped lee waves applying momentum budgets locally, but, as pointed out earlier herein, they used for that purpose purely inviscid theory. An extension of the present quasi-inviscid theory would allow this to be done in a more physically consistent way. Meanwhile, as a practical compromise, the drag force that the present theory predicts to act over the whole region spanned by the waves could be distributed uniformly over the grid points included in that region, thereby producing an at least globally accurate impact.

The Rayleigh damping approach adopted to represent friction in the present study may be viewed as non-optimal, due to its crudeness and specificity. However, the independence of the quasi-inviscid results from λ and their agreement with the inviscid numerical simulations suggest that they may be more general than expected. Except within the atmospheric boundary layer, friction in a stratified atmosphere is typically quite weak, and this is also corroborated by the large horizontal extent of trapped lee waves that can be visualized through cloud condensation in satellite images. For these reasons, there is scope to believe that the results presented here may constitute a good basis for the development of new physically based drag parametrizations for trapped lee waves.

AUTHOR CONTRIBUTIONS

Miguel A. C. Teixeira: conceptualization; formal analysis; investigation; methodology; visualization; writing – original draft; writing – review and editing. **José L. Argaín:** conceptualization; data curation; investigation; methodology; resources; software; validation.

ORCID

Miguel A. C. Teixeira https://orcid.org/0000-0003-1205-3233
José L. Argaín https://orcid.org/0000-0001-9140-0867

REFERENCES

Argaín, J.L. (2003). Numerical modelling of atmospheric flow: Orographic and boundary layer effects (PhD thesis). University of Algarve, Faro, Portugal.

Argaín, J.L., Miranda, P.M.A. and Teixeira, M.A.C. (2009) Estimation of the friction velocity in stably stratified boundary-layer flows over hills. *Boundary-Layer Meteorology*, 130, 15–28.

Argaín, J.L., Teixeira, M.A.C. and Miranda, P.M.A. (2017) Estimation of surface-layer scaling parameters in the unstable boundary layer: Implications for orographic flow speed-up. *Boundary-Layer Meteorology*, 165, 145–160.

Booker, J.R. and Bretherton, F.P. (1967) The critical layer for internal gravity waves in a shear flow. *Journal of Fluid Mechanics*, 27, 513–539.

Bretherton, F.P. (1969) Momentum transport by gravity waves. *Quarterly Journal of the Royal Meteorological Society*, 95, 213–243.

Broad, A.S. (2002) Momentum flux due to trapped lee waves forced by mountains. *Quarterly Journal of the Royal Meteorological Society*, 128, 2167–2173.

Corby, G.A. and Wallington, C.E. (1956) Airflow over mountains: The lee wave amplitude. *Quarterly Journal of the Royal Meteorological Society*, 82, 266–274.

Durran, D.R. (1995) Do breaking mountain waves decelerate the local mean flow?. *Journal of the Atmospheric Sciences*, 52, 4010–4032.

Eliassen, A. and Palm, E. (1960) On the transfer of energy in stationary mountain waves. *Geofysiske Publikasjoner*, 22, 1–23.

Gregory, D., Shutts, G.J. and Mitchell, J.R. (1998) A new gravity-wave-drag scheme incorporating anisotropic orography and low-level wave breaking. Impact upon the climate of the UK Meteorological Office Unified Model. *Quarterly Journal of the Royal Meteorological Society*, 124, 463–493.

Grubišić, V. and Smolarkiewicz, P.K. (1997) The effect of critical levels on 3D orographic flows: Linear regime. *Journal of the Atmospheric Sciences*, 54, 1943–1960.

Jiang, Q., Doyle, J.D. and Smith, R.B. (2006) Interaction between trapped waves and boundary layers. *Journal of the Atmospheric Sciences*, 63, 617–633.

Lin, Y.-L. (2007) *Mesoscale dynamics*. New York; NY: Cambridge University Press.

Lott, F. (1998) Linear mountain drag and averaged pseudo-momentum flux profiles in the presence of trapped-lee waves. *Tellus A*, 50, 12–25.

Lott, F. (2007) The reflection of a stationary gravity wave by a viscous boundary layer. *Journal of the Atmospheric Sciences*, 64, 3363–3371.

Lott, F. and Miller, M.J. (1997) A new subgrid-scale orographic drag parametrization: Its formulation and testing. *Quarterly Journal of the Royal Meteorological Society*, 123, 101–127.

McFarlane, N.A. (1987) The effect of orographically excited gravity-wave drag on the general circulation of the lower stratosphere and troposphere. *Journal of the Atmospheric Sciences*, 44, 1775–1800.

Mitchell, R.M., Cechet, R.P., Turner, P.J. and Elsum, C.C. (1990) Observation and interpretation of wave clouds over Macquarie Island. *Quarterly Journal of the Royal Meteorological Society*, 116, 741–752.

Nance, L.B. and Durran, D.R. (1998) A modelling study of non-stationary trapped mountain lee waves. Part II: Nonlinearity. *Journal of the Atmospheric Sciences*, 55, 1429–1445.

Nappo, C.J. (2012) *An introduction to atmospheric gravity waves* (2nd). Waltham, MA: Academic Press.

Phillips, D.S. (1984) Analytical surface pressure and drag for linear hydrostatic flow over three-dimensional elliptical mountains. *Journal of the Atmospheric Sciences*, 41, 1073–1084.

Scorer, R.S. (1949) Theory of waves in the lee of mountains. *Quarterly Journal of the Royal Meteorological Society*, 75, 41–56.

Shepherd, T.G. (1990) Symmetries; conservation laws; and Hamiltonian structure in geophysical fluid dynamics. *Advances in Geophysics*, 32, 287–338.

Shutts, G. (1995) Gravity-wave drag parametrization over complex terrain: The effect of critical-level absorption in directional wind-shear. *Quarterly Journal of the Royal Meteorological Society*, 121, 1005–1021.

Shutts, G.J. and Gadian, A. (1999) Numerical simulations of orographic gravity waves in flows which back with height. *Quarterly Journal of the Royal Meteorological Society*, 125, 2743–2765.

Smith, R.B. (1976) The generation of lee waves by the Blue Ridge. *Journal of the Atmospheric Sciences*, 33, 507–519.

Smith, R.B. (1979) The influence of mountains on the atmosphere. *Advances in Geophysics*, 21, 87–230.

Smith, R.B., Jiang, Q. and Doyle, J.D. (2006) A theory of gravity wave absorption by a boundary layer. *Journal of the Atmospheric Sciences*, 63, 774–781.

Soufflet, C., Lott, F. and Deremble, B. (2022) Mountain waves produced by a stratified flow with a boundary layer. Part III: Trapped lee waves and horizontal momentum transport. *Journal of the Atmospheric Sciences*, 9, 1601–1614.

Stensrud, D.J. (2009) *Parametrization schemes: Keys to understanding numerical weather prediction models*. New York, NY: Cambridge University Press.

Teixeira, M.A.C., Argaín, J.L. and Miranda, P.M.A. (2012) The importance of friction in mountain wave drag amplification by scorer parameter resonance. *Quarterly Journal of the Royal Meteorological Society*, 138, 1325–1337.

Teixeira, M.A.C., Argaín, J.L. and Miranda, P.M.A. (2013a) Drag produced by trapped lee waves and propagating mountain and propagating mountain waves in a two-layer atmosphere. *Quarterly Journal of the Royal Meteorological Society*, 139, 964–981.

Teixeira, M.A.C., Argaín, J.L. and Miranda, P.M.A. (2013b) Orographic drag associated with lee waves trapped at an inversion. *Journal of the Atmospheric Sciences*, 70, 2930–2947.

Teixeira, M.A.C. and Miranda, P.M.A. (2006) A linear model of gravity wave drag for hydrostatic sheared flow over elliptical mountains. *Quarterly Journal of the Royal Meteorological Society*, 132, 2439–2458.

Teixeira, M.A.C. and Miranda, P.M.A. (2009) On the momentum fluxes associated with mountain waves in directionally sheared flows. *Journal of the Atmospheric Sciences*, 66, 3419–3433.

Teixeira, M.A.C. and Miranda, P.M.A. (2017) Drag associated with 3D trapped lee waves over an axisymmetric obstacle in two-layer atmospheres. *Quarterly Journal of the Royal Meteorological Society*, 143, 3244–3258.

Teixeira, M.A.C., Miranda, P.M.A. and Argaín, J.L. (2008) Mountain waves in two-layer sheared flows: Critical level effects; wave reflection and drag enhancement. *Journal of the Atmospheric Sciences*, 65, 1912–1926.

Teixeira, M.A.C., Miranda, P.M.A. and Valente, M.A. (2004) An analytical model of mountain wave drag for wind profiles with shear and curvature. *Journal of the Atmospheric Sciences*, 61, 1040–1054.

Teixeira, M.A.C. and Yu, C.L. (2014) The gravity wave momentum flux in hydrostatic flow with directional shear over elliptical mountains. *European Journal of Mechanics – B/Fluids*, 47, 16–31.

Turner, H.V., Teixeira, M.A.C. and Methven, J. (2021) The effect of a stable boundary layer on orographic gravity wave drag. *Quarterly Journal of the Royal Meteorological Society*, 147, 321–340.

Vosper, S.B., Sheridan, P.F. and Brown, A.R. (2006) Flow separation and rotor formation beneath two-dimensional trapped lee waves. *Quarterly Journal of the Royal Meteorological Society*, 132, 2415–2438.

Xu, X., Li, R., Teixeira, M.A.C. and Lu, Y. (2021) On the momentum flux of vertically propagating orographic gravity waves excited in nonhydrostatic flow over three-dimensional orography. *Journal of the Atmospheric Sciences*, 78, 1807–1822.

Xue, H. and Giorgietta, M.A. (2021) A large-eddy simulation study on the diurnally evolving nonlinear trapped lee waves over a two-dimensional steep mountain. *Journal of the Atmospheric Sciences*, 78, 399–415.

Xue, H., Giorgietta, M.A. and Guo, J. (2022) The daytime trapped lee wave pattern and evolution induced by two small-scale mountains of different heights. *Quarterly Journal of the Royal Meteorological Society*, 148, 1300–1318.

How to cite this article: Teixeira, M.A.C. & Argaín, J.L. (2022) The drag exerted by weakly dissipative trapped lee waves on the atmosphere: Application to Scorer's two-layer model. *Quarterly Journal of the Royal Meteorological Society*, 148(748), 3211–3230. Available from: https://doi.org/10.1002/qj.4355

APPENDIX A. DERIVATION OF IMPORTANT EQUATIONS

A.1 Obtaining Equation (12) from Equations (10) and (11)

If Equation (11) is multiplied by u or w and differentiated with respect to x or z respectively, the following two equations are obtained:

$$\frac{\partial}{\partial x}\left(\frac{pu}{\rho_0}\right) = -U\frac{\partial}{\partial x}\left(u^2\right) - U\frac{dU}{dz}\frac{\partial}{\partial x}(\zeta u) - \lambda u^2 - \lambda\frac{\partial u}{\partial x}\int^x u\,dx, \tag{A1}$$

$$\frac{\partial}{\partial z}\left(\frac{pw}{\rho_0}\right) = -U\frac{\partial}{\partial z}(uw) - uw\frac{dU}{dz} - \frac{dU}{dz}\frac{\partial}{\partial z}(U\zeta w) - U\frac{d^2U}{dz^2}\zeta w - \lambda w\int^x \frac{\partial u}{\partial z}\,dx - \lambda\frac{\partial w}{\partial z}\int^x u\,dx. \tag{A2}$$

Adding these two equations yields

$$\frac{\partial}{\partial x}\left(\frac{pu}{\rho_0}\right) + \frac{\partial}{\partial z}\left(\frac{pw}{\rho_0}\right) = -U\frac{\partial}{\partial x}\left(u^2\right) - U\frac{\partial}{\partial z}(uw) - uw\frac{dU}{dz} - U\frac{d^2U}{dz^2}\zeta w - \lambda u^2 - \lambda w\int^x \frac{\partial u}{\partial z}\,dx. \tag{A3}$$

To simplify this equation, we used the mass conservation Equation (9) in the last terms of Equations (A1) and (A2), and also the fact that

$$\begin{aligned} U\frac{\partial}{\partial x}(\zeta u) + \frac{\partial}{\partial z}(U\zeta w) &= -U\frac{\partial}{\partial x}\left[\zeta\frac{\partial}{\partial z}(U\zeta)\right] + w\frac{\partial}{\partial z}(U\zeta) + U\zeta\frac{\partial w}{\partial z} \\ &= -U\frac{\partial \zeta}{\partial x}\frac{\partial}{\partial z}(U\zeta) - U\zeta\frac{\partial^2}{\partial x\partial z}(U\zeta) + U\frac{\partial \zeta}{\partial x}\frac{\partial}{\partial z}(U\zeta) \\ &\quad + U\zeta\frac{\partial w}{\partial z} = U\zeta\frac{\partial u}{\partial x} + U\zeta\frac{\partial w}{\partial z} = 0, \end{aligned} \tag{A4}$$

which implies that the sum of the second term on the right-hand side of Equation (A1) and the third term on the right-hand side of Equation (A2) cancel out. Equation (A4) uses the fact that $w = U\partial\zeta/\partial x$, and also that, by Equation (9), $u = -\partial(U\zeta)/\partial x$. Then, inserting Equation (A3) into Equation (10), the latter becomes

$$U\frac{\partial}{\partial x}\left(\frac{u^2+w^2}{2}\right) - U\frac{\partial}{\partial x}\left(u^2\right) - U\frac{\partial}{\partial z}(uw) - U^2\frac{d^2U}{dz^2}\zeta\frac{\partial \zeta}{\partial x} - \lambda w\int^x \frac{\partial u}{\partial z}\,dx + N^2U\zeta\frac{\partial \zeta}{\partial x} + \lambda w^2 = 0, \tag{A5}$$

where the terms with $uw(dU/dz)$ and λu^2 cancelled out and $w = U\partial\zeta/\partial x$ has been used. This can be simplified further by expressing $\zeta\partial\zeta/\partial x = (1/2)\partial(\zeta^2)/\partial x$, grouping the second, fourth, and sixth terms on the left-hand side of Equation (A5) with the first term and noting that $w = \int^x (\partial w/\partial x)\, dx$. This finally yields Equation (12).

A.2 Obtaining Equation (23) from Equation (12)

If Equation (12) is integrated between $-\infty$ and $+\infty$ in a situation when $\lambda \neq 0$, the following results:

$$
\begin{aligned}
U\frac{\partial}{\partial z}\int_{-\infty}^{+\infty} uw\, dx &= -\lambda\int_{-\infty}^{+\infty} w\int^{x}\left(\frac{\partial u}{\partial z} - \frac{\partial w}{\partial x}\right) dx'\, dx \\
&= -\lambda U\int_{-\infty}^{+\infty} \frac{\partial \zeta}{\partial x}\int^{x}\left(\frac{\partial u}{\partial z} - \frac{\partial w}{\partial x}\right) dx'\, dx \\
&= \lambda U\int_{-\infty}^{+\infty} \zeta\left(\frac{\partial u}{\partial z} - \frac{\partial w}{\partial x}\right) dx,
\end{aligned}
\tag{A6}
$$

where the second equality used $w = U\partial\zeta/\partial x$ and the third one used integration by parts. Equation (A6) is equivalent to Equation (21). Dividing this equation by U and integrating in the vertical between a generic z and $+\infty$ (where $uw = 0$) yields Equation (22), reproduced here:

$$
\int_{-\infty}^{+\infty} uw\, dx = -\lambda\int_{z}^{+\infty}\int_{-\infty}^{+\infty} \zeta\left(\frac{\partial u}{\partial z} - \frac{\partial w}{\partial x}\right) dx\, dz. \tag{A7}
$$

The last step requires using the equalities $w = U\partial\zeta/\partial x$ and $u = -\partial(U\zeta)/\partial z$, yielding

$$
\begin{aligned}
\int_{-\infty}^{+\infty} uw\, dx &= \lambda\int_{z}^{+\infty}\int_{-\infty}^{+\infty} \zeta\left[\frac{\partial^2}{\partial z^2}(U\zeta) + U\frac{\partial^2\zeta}{\partial x^2}\right] dx\, dz \\
&= \lambda\int_{z}^{+\infty} U\int_{-\infty}^{+\infty} \zeta\left(\frac{\partial^2\zeta}{\partial x^2} + \frac{\partial^2\zeta}{\partial z^2} + \frac{2}{U}\frac{dU}{dz}\frac{\partial\zeta}{\partial z} + \frac{1}{U}\frac{d^2U}{dz^2}\zeta\right) \\
&\quad \times dx\, dz.
\end{aligned}
\tag{A8}
$$

Finally, assuming that λ is small enough, the inviscid version of the wave equation that is valid in this case (Lin, 2007, eq. (5.3.1), neglecting the nonlinear term),

$$
\frac{\partial^2\zeta}{\partial x^2} + \frac{\partial^2\zeta}{\partial z^2} + \frac{2}{U}\frac{dU}{dz}\frac{\partial\zeta}{\partial z} + \frac{N^2}{U^2}\zeta = 0, \tag{A9}
$$

may be inserted into Equation (A8), yielding

$$
\int_{-\infty}^{+\infty} uw\, dx = \lambda\int_{z}^{+\infty} U\int_{-\infty}^{+\infty} \zeta\left(-\frac{N^2}{U^2}\zeta + \frac{1}{U}\frac{d^2U}{dz^2}\zeta\right) dx\, dz. \tag{A10}
$$

This is equivalent to Equation (23).